1 **Comparative study of alteration sequences in pegmatitic aluminium phosphates**

2

3 Cassian Pirard[1,2,3]

4 *1. Laboratoire de Minéralogie et de Cristallochimie, Département de Géologie, Université de*

5 *Liege, Liege, Belgium*

6 *2. Research School of Earth Sciences, College of Science, Australian National University,*

7 *Canberra, Australia*

8 *3. EGRU, Earth & Environmental Sciences, College of Science and Engineering, James Cook*

9 *University, Townsville, Australia.*

10

11 *corresponding author: cassian.pf.pirard@gmail.com*

12

13

14

15

16

17

18 **Foreword**

19   This document is a draft that might be published in the future with additional co-authors.

20 Considering the interest regarding a poster presented at an International Symposium in Porto in

21 2007, it seems appropriate to provide a full dataset in English on this subject. This draft is not peer-

22 reviewed so data and interpretation should be exploited carefully.

23

24

25

26   **1. <u>Abstract</u>**

27   Aluminium phosphates are mineral phases commonly occurring in rare-element pegmatites

28 that record initial magmatic crystallization, metasomatic and hydrothermal replacements and

29 precipitation and low-temperature alteration. Here we perform a comparative mineralogical study

30 between several localities to assess similarities and variations in these parageneses and establish a

31 general alteration sequence of such mineral assemblages.

32

33 Keywords: Pegmatite, aluminium phosphates, amblygonite-montebrasite, alteration, Montebras,

34 Karibib, Gatumba

35

36

37

38   **<u>Résumé</u>**

39

40   Les phosphates d'aluminium sont des phases minérales communément présentes dans les

41 pegmatites à éléments rares qui enregistrent la cristallisation magmatique initiale, les

42 remplacements et précipitations métasomatiques et hydrothermales et l'altération à basse

43 temperature. Dans la présente étude, nous entreprenons une étude minéralogique comparative de

44 plusieurs localités pour estimer les similitudes et variations des paragéneses et établir une séquence

45 d'altération approximative pour de tels assemblages minéraux.

46

47 Mots-clés: Pegmatite, phosphates d'aluminium, amblygonite-montebrasite, Montebras, Karibib,

48 Gatumba

49

50

51 **1. <u>Introduction</u>**

52

53   Phosphate minerals in granitic pegmatite environments often shows a complex assemblage of

54 phosphates containing alkali and transition metals (Moore, 1973). Despite being a minor constituent

55 in igneous environments, the information carried by phosphates in the post-magmatic history of an

56 intrusion is considerable due to their sensitivity to geochemical conditions (oxidation, hydration,

57 leaching and metasomatism) upon cooling that leads to the recrystallization of a multitude of

58 secondary phosphates (Mason, 1941; Moore, 1982; Fransolet, 2007).

59   Primary and secondary phosphate mineralogy and parageneses have been extensively studied in

60 granitic pegmatite environments for mineralogical and petrogenetic purposes. However, most of

61 these studies focused on Fe-Mn phosphates, which are particularly sensitive to geochemical

62 changes and form minerals with remarkable optical properties. On the other hand, many Fe-Mn-free

63 aluminium phosphates tend to occur as inconspicuous white or colourless phases with uneventful

64 optical characteristics that has hindered some initial petrological studies on these materials and their

65 petrogenetic value neglected.

66   Here, we provide a characterization of phosphate assemblages in different pegmatites (France,

67 Rwanda, Namibia) where Fe-Mn phosphates are rare in order to document and compare variations

68 in the primary cristallisation and alteration sequences of secondary aluminium phosphates

69 assemblages in the post-magmatic environment and the possible influence of meteoric factors

70 caused by different climate conditions.

71

72

73

74

75

76 **2. <u>Geological background</u>**

77

78 **2.1 Montebras-en-Soumans (France)**

79

80 The Montebras pegmatite is a famous locality-type deposit in the Massif Central, France

81 [N46º19'16'', E2º17'46'']. It lies on the northwest margin of the Hercynian belt where a

82 microgranite intruded a granite batholith, forming a cupola of albite leucogranite where a pegmatite

83 is found. The typical pegmatite facies (stockscheider) mostly contain K-feldspar with some quartz,

84 albite, muscovite, apatite and some amblygonite-montebrasite, as well as rare cassiterite and some

85 turquoise pods. The second facies (quartzglöcke) is quartz-rich with K-feldspar, micas, large

86 aggregates of cassiterite, blue apatite and large masses of Al-rich phosphates (Moissenet, 1871;

87 Aubert, 1969). Samples used in this study come mostly from the quartzglöcke and are part of

88 collections at the University of Liege and the School of Mines of Paris, including original samples

89 from Alfred Lacroix (Lacroix, 1891; 1910). The phosphate mineralogical description of this deposit

90 is described in Pirard (2022) and samples are labelled as 'MONT'.

91

92 **2.2. Gatumba District (Rwanda)**

93

94 Bwimo-Nyarusange pegmatite is a minor altered cassiterite deposit in the Gatumba district,

95 Rwanda [S1º56' – E29º41']. It is listed as a spodumene-amblygonite pegmatite intrusion. The

96 eluvial deposit has produced a few tons of tin (BRGM, 1987).

97 The Gatumba district is a Mesoproterozoic metasedimentary unit resulting from the Kibaran

98 orogeny. The district contains large granitic intrusions where the most differentiated alkaline

99 granites are dated at 976 Ma (Cahen and Ledent, 1979). The samples from Bwimo were collected in

100 1983 by Prof. André-Mathieu Fransolet (ULiege) from the mine tailing and are altered masses of

101 montebrasite as well as some sample of cassiterite-rich microcline blocks. Samples are labelled as

102 'BW'.

103

104   **2.3. Karibib District (Namibia)**

105

106   The third group of samples come from 3 pegmatite bodies (Helikon I (Okongava Ost Farm),

107 Habis Farm, McDonalds (Etusis Farm)) in Karibib, Namibia [resp. S22º1'36''-E16º1'0''; S22º09' –

108 E15º48'; S22º07' – E15º34'] (Diehl, 1992). The pegmatite bodies were mined for amblygonite,

109 petalite and lepidolite as well as accessory pollucite, Mn-columbite, beryl and quartz (Keller, 1991).

110   This pegmatite field is intruded in a metasedimentary basement formed during the

111 Neoproterozoic Damaran orogeny. Numerous syn- and post- tectonic granites are present and

112 associated with pegmatite bodies concordant with the metamorphic host-rock. Samples used in this

113 study were collected by Prof. Paul Keller (Universität Stuttgart) in the outer part of the quartz-core

114 of these pegmatite bodies and described as massive white amblygonite. Samples are labelled as

115 'KBB'

116

117

118

119

120

121

122

123

124

125

126   **3. <u>Analytical techniques</u>**

127

128   Samples were extensively studied with a binocular lens and optical microscope Leica DMLP at

129   the Laboratory of Mineralogy and Crystallography (ULiege). However, issues arising in the

130   standard microscopical study of aluminium phosphates led us to perform many microscopic

131   observations with cathodoluminescence (see Pirard, 2022). Paragenesis and textural determination

132   were mostly determined using an Olympus BX50 microscope and a CITL cold cathode

133   luminescence 8200 mk3 housed by the EDDyLab (ULiege). Observations were made at 0.05 mbar

134   with an electronic current of 15±2 kV and 700±50 μA. Cathodoluminescence spectra were obtained

135   with a hot cathode system on a JEOL JXA8200 at the Advanced Analytical Centre (JCU) and

136   processed with XCLent software.

137   Identification of less common mineral species was done using X-ray diffraction (XRD) using a

138   Philips PW-3710 diffractometer with a graphite monochromator and a CuKα (λ = 1.5418 Å) or

139   FeKα (λ = 1.9373 Å) radiation source at the Laboratory of Mineralogy and Crystallography (ULg).

140   For microscopic grains, XRD was done on a Debye-Scherrer camera (diameter = 114.6 mm)

141   mounted on the same X-ray sources. Unit-cell parameters were calculated through least-square

142   refinement program LCLSQ v.8.4 (Burnham, 1991), using *d* values corrected on an internal

143    $Pb(NO_3)_2$ standard.

144   Chemical analyses were mostly done using electron microprobe CAMECA SX-50 (Ruhr-

145   Universität Bochum) with 15 kV and 8 nA conditions with a 10 μm beam diameter. Standard were

146   jadeite (Na), synthetic glasses (K, Ba), spessartine (Al, Mn), andradite (Si, Fe, Ca), graftonite (P),

147    $SrCu_4Si_4O_{10}$ (Sr, Cu), pyrope (Mg) and topaz (F). The counting time per element is 30 s and 15 s for

148   the most beam-sensitive phases. Fluorine has a 120 s counting time on a PC0 crystal. Beam-

149   sensitive phases analyses were doubled checked with a JEOL 6400 SEM at the Electron Microscopy

150   Unit (ANU) with an EDS system calibrated on known mineral standards, operating at 15 kV, 1 nA

151   with a 1 μm beam diameter with 120 s counting time. Fluorine in lacroixite, apatite, morinite and

152   phase F have been analysed on JEOL JXA8200 at the Advanced Analytical Centre (JCU) using a 15

153   kV acceleration voltage, 14.5 nA current. Fluorine is measured using a time-zero integrated analysis

154   where FKα is monitored for 35 s on TAP crystal and regressed to provide an initial value.

155   Trace element data was obtained using a laser ablation inductively coupled plasma mass

156   spectrometry (LA-ICP-MS) at the Research School of Earth Science (RSES, ANU), using a pulsed

157   193 mm ArF Excimer laser with 3-7 mJ of output energy reaching the sample at a repetition rate of

158   5 Hz (Eggins et al., 1998), coupled to an Agilent HP7500 quadrupole ICP-MS system. Laser

159   sampling was perfomed in an Ar atmosphere with He:H_2 (ratio 15:1) as a carrier gas with a beam

160   size of 30-50 μm in diameter. ^{27}Al was the internal standard and NIST SRM 612 glass an external

161   standard with reference from Spandler et al. (2011). BCR-2G glass was used as a secondary

162   standard and reproductibility was better than 7%.

163   Infrared spectra were obtained on a Nicolet Nexus at the Laboratory of Mineralogy and

164   Crystallography (ULg) between 400 and 4000 cm^{-1} through 32 scans with a 1 cm^{-1} resolution.

165   Infrared source is heated SiC (Ever-Glo). Samples were prepared through a mixture with KBr (1:74)

166   producing a 150 mg pressed pellet dried at 110ºC and analysed in a dry atmosphere.

167

168

169   **4.   Mineral characterisation**

170

171   **4.1.   Lithium phosphates**

172

173   Amblygonite-Montebrasite series [*LiAl(PO$_4$)(F,OH)*] - This mineral series is the

174   dominant primary phase in phosphate assemblages of all studied localities. It occurs as light-

175   coloured centimetre-sized idiomorphic crystals but is almost constantly altered by quartz,

176   lacroixite, apatite and hydrous phosphates. In all deposits, primary amblygonite is often

177   replaced by secondary montebrasite (rarely amblygonite) in lamellae along cleavage, twinning

178   planes (Fig 1a.) and cracks while a tertiary montebrasite is observed in veinlets (Fig. 1b)

179   crossing first and second generations of amblygonite-montebrasite in all localities but only fresh

180   in Montebras, Helikon I and McDonalds. The presence of two or more generations of

181   amblygonite-montebrasite is frequently described in many similar deposits (Pirard, 2022;

182   Shirose & Uehara, 2014; Galliski et al., 2012; Scholz et al., 2008; London & Burt, 1982).
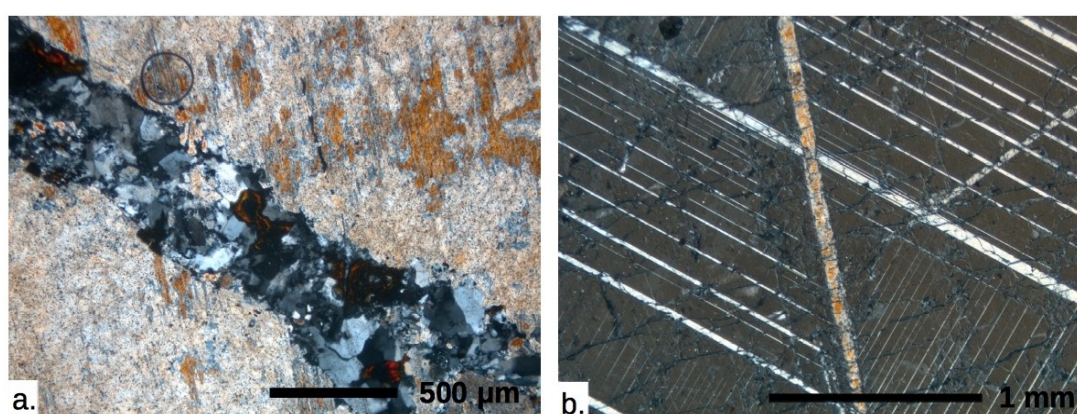
184   Figure 1. a. Primary amblygonite (beige) with replacement by secondary amblygonite (orange). Late quartz vein (grey) with

185   varlamoffite (red-brown) and crandallite-goyazite (grey) in crossed polarised light. Sample MONT 9. b. Primary amblygonite with

186   polysynthetic twinning, minor secondary amblygonite and two veins of tertiary montebrasite seen in crossed polarised light. Sample

187   BW5.
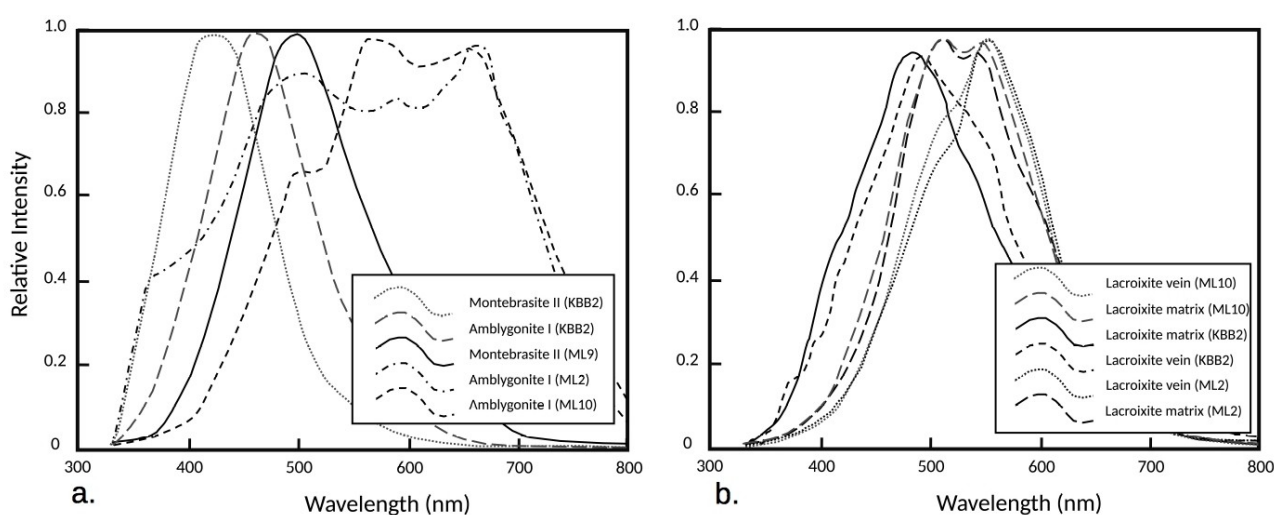
188   Figure 2. a. Cathodoluminescence spectra of primary (I) and secondary (II) amblygonite-montebrasite in sample KBB2, MONT2,

189   MONT 9 and MONT10. b. Cathodoluminescence spectra of lacroixite veins and meshy lacroixite (matrix) in sample KBB2, MONT2

190   and MONT10.
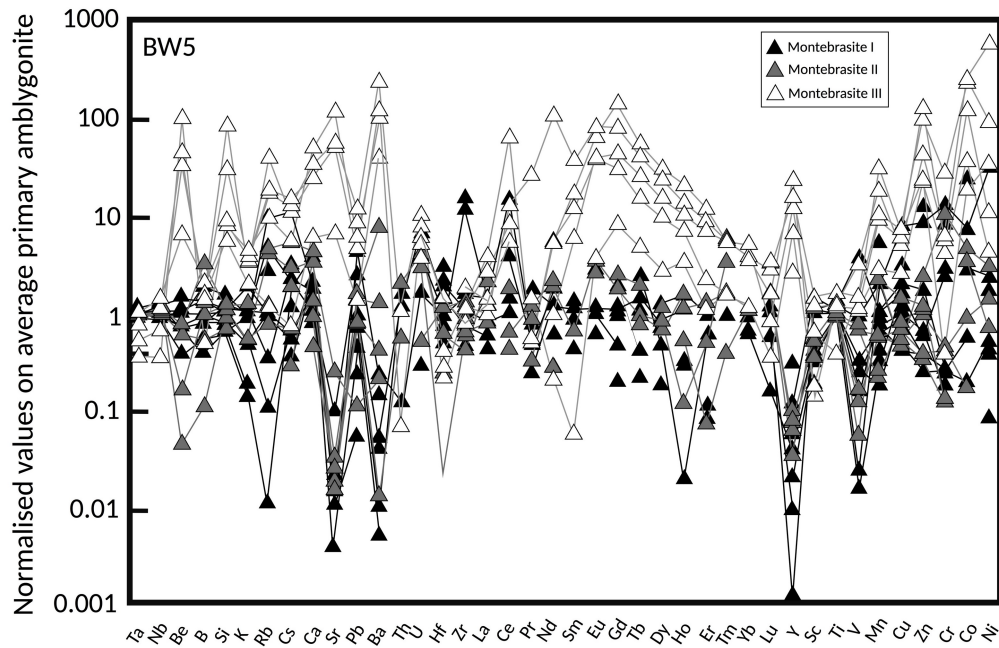
191   Figure 3. Example of trace element concentrations in amblygonite-montebrasite normalised on the average primary amblygonite free

192   of any inclusions. Variations in concentration of trace elements are mild for secondary montebrasite and mostly systematically

193   enriched for tertiary montebrasite in sample BW5.

194

195   Cathodoluminescence spectra of amblygonite-montebrasite is not systematic although

196   differences between the three generations can be observed (Fig. 2a). Trace elements

197   concentrations changes from sample to sample but show relatively systematic patterns within

198   each samples between the different generations of $LiAlPO_4(F,OH)$. Tertiary montebrasite veins

199   have a particularly differentiated REE pattern and high concentrations in LILE and transition

200   metals (Fig. 3). Electron probe micro-analysis shows high fluorine content for primary

201   amblygonite (Montebras: >10 wt.% F; Karibib: ~8 wt.% F; Bwimo: 4 wt.% F (Table 1)).

202   Secondary amblygonite-montebrasite ranges from 6 to 3 wt.% F in Montebras and Karibib

203   while secondary montebrasite in Bwimo is below 3 wt.% F. The tertiary montebrasite is an

204   hydroxyl-rich montebrasite below 2.5 wt.% F (Table 1, Fig. 4).

205

206

207

208

209

210

211

212

213

214   Figure 4. Distribution of analyses in different samples of each localities for different generations. Vertical lines is the standard

215   deviation for each generation. Primary (I) amblygonite in Montebras and Karibib are high in fluorine while Bwimo shows lower

216   content. Secondary (II) and Tertiary (III) amblygonite-montebrasite show lower fluorine content with the decrease in fluorine

217   consistent in each sample.

218

219

220

221

222

223

224

Table 1. Composition of amblygonite-montebrasite (Bwimo, Karibib)

Sample	BW1	BW1	BW3	BW5	BW5	BW7	KBB1	KBB1	KBB1	KBB2	KBB2	KBB3	KBB3	KBB3
phase	I	II		I	II		I	II	III	I	II	I	II	III
n	8	4	5	4	9	7	6	8	5	6	3	1	3	3
P_2O_5	50.62 (57)	50.65 (102)	50.44 (71)	51.30 (101)	50.47 (80)	50.88 (61)	49.29 (39)	49.71 (58)	50.90 (130)	50.40 (56)	50.16 (15)	50.62	50.05 (41)	48.75 (273)
Al_2O_3	34.93 (77)	34.67 (17)	35.20 (32)	34.90 (25)	34.95 (40)	35.08 (37)	34.48 (16)	34.56 (16)	34.73 (56)	35.17 (12)	34.67 (7)	34.55	34.38 (9)	34.43 (199)
Na_2O	bdl	tr.	bdl	bdl	bdl	bdl	0.14 (8)	bdl	0.05 (4)	tr.	tr.	bdl	bdl	bdl
F	3.87 (46)	2.24 (24)	1.97 (115)	2.22 (23)	2.69 (7)	2.67 (9)	9.72 (50)	5.51 (28)	1.36 (18)	8.25 (44)	4.04 (136)	6.80	4.66 (26)	2.53 (2)
Li_2O	10.50 (14)	10.43 (17)	10.50 (8)	10.58 (16)	10.48 (13)	10.55 (8)	10.21 (5)	10.34 (8)	10.49 (23)	10.49 (7)	10.40 (3)	10.46	10.35 (6)	10.17 (62)
H_2O	4.50 (21)	5.25 (18)	5.40 (58)	5.33 (19)	5.04 (7)	5.09 (7)	1.59 (21)	3.62 (14)	5.70 (15)	2.42 (22)	4.36 (65)	3.08	4.04 (9)	4.95 (34)
Total	104.41 (151)	103.34 (86)	103.53 (64)	104.35 (131)	103.64 (124)	104.28 (73)	105.42 (84)	103.75 (79)	103.22 (210)	106.74 (61)	103.65 (66)	105.51	103.51 (74)	100.89 (561)
Total O =F	102.79 (144)	102.39 (96)	102.70 (70)	103.42 (140)	102.51 (122)	103.15 (73)	101.33 (65)	101.43 (78)	102.65 (209)	103.26 (62)	101.95 (19)	102.65	101.54 (63)	99.82 (560)
P	1.02 (1)	1.02 (1)	1.01 (1)	1.01 (1)	1.02 (1)	1.02 (1)	1.01 (0)	1.01 (0)	1.02 (1)	1.01 (0)	1.01 (0)	1.02	1.02 (0)	1.01 (0)
Al	0.97 (1)	0.97 (2)	0.98 (1)	0.98 (1)	0.97 (1)	0.97 (1)	0.98 (0)	0.98 (1)	0.97 (1)	0.98 (1)	0.98 (0)	0.97	0.97 (0)	0.99 (0)
Na	bdl	tr.	bdl	bdl	bdl	0.00 (0)	0.01 (0)	bdl	tr.	tr.	tr.	bdl	bdl	0.00 (0)
F	0.29 (3)	0.17 (2)	0.15 (9)	0.20 (0)	0.16 (2)	0.20 (1)	0.74 (4)	0.42 (2)	0.10 (1)	0.62 (3)	0.31 (10)	0.51	0.35 (2)	0.20 (1)
Li	1.00 (0)	1.00 (1)	1.00 (0)	1.00 (0)	1.00 (0)	1.00 (0)	0.99 (0)	1.00 (0)	1.00 (0)	1.00 (0)	1.00 (0)	1.00	1.00 (0)	1.00 (0)
OH	0.71 (3)	0.83 (2)	0.85 (9)	0.80 (0)	0.84 (2)	0.80 (1)	0.26 (4)	0.58 (2)	0.90 (1)	0.38 (3)	0.69 (10)	0.49	0.65 (2)	0.80 (1)
Σcat.	2.99 (0)	2.99 (1)	2.99 (0)	2.99 (0)	2.99 (0)	2.99 (0)	2.99 (0)	2.99 (0)	2.99 (0)	2.99 (0)	2.99 (0)	2.99	2.99 (0)	3.00 (0)
F/(F+OH)	0.29 (3)	0.17 (2)	0.15 (9)	0.20 (0)	0.16 (2)	0.20 (1)	0.74 (4)	0.42 (2)	0.10 (1)	0.62 (3)	0.31 (10)	0.51	0.35 (2)	0.20 (1)

Amblygonite-Montebrasite calculated on 4 oxygens - Hydroxyls calculated by difference on fluorine site (1-F) - Li calculated by difference of Na on lithium site (1-Na)

Table 1. Composition of amblygonite-montebrasite (Montebras)

Sample	MONT2	MONT2	MONT3	MONT5	MONT9	MONT9	MONT9	MONT10	MONT10	MONT10	MONT13	MONT14	MONT15	MONT15	ML19
phase	I	II			I	II	III	8	6	3	4	6	I	II	8
n	7	4	6	6	3	7	3	8	6	3	4	6	1	4	8
P_2O_5	49.22 (43)	49.83 (104)	49.95 (39)	50.79 (60)	50.17 (31)	49.44 (105)	50.79 (104)	50.04 (63)	49.59 (43)	50.18 (45)	50.20 (65)	50.22 (70)	49.97	49.92 (148)	46.02 (68)
Al_2O_3	34.42 (20)	34.45 (35)	34.67 (5)	34.89 (14)	34.32 (13)	34.78 (50)	34.51 (33)	34.86 (26)	34.44 (16)	35.13 (20)	34.75 (15)	35.27 (19)	34.74	34.97 (18)	31.64 (89)
Na_2O	0.80 (70)	1.44 (90)	tr.	bdl	bdl	bdl	bdl	0.11 (6)	0.13 (6)	0.11 (2)	bdl	tr.	bdl	bdl	bdl
F	9.90 (42)	6.59 (143)	10.64 (20)	5.64 (69)	3.63 (30)	1.77 (19)	0.78 (12)	10.69 (9)	9.52 (52)	5.88 (58)	10.03 (50)	4.00 (48)	10.42	4.60 (46)	3.29 (39)
Li_2O	9.87 (39)	9.65 (57)	10.35 (7)	10.49 (11)	10.36 (3)	10.31 (17)	10.47 (15)	10.36 (8)	10.25 (8)	10.41 (8)	10.41 (8)	10.42 (12)	10.39	10.41 (20)	9.52 (19)
H_2O	1.49 (20)	3.11 (75)	1.21 (7)	3.67 (34)	4.53 (13)	5.38 (13)	5.94 (9)	1.21 (7)	1.70 (24)	3.52 (27)	1.53 (21)	4.43 (23)	1.33	4.09 (26)	4.19 (26)
														(0)	
Total	105.70 (43)	105.06 (89)	106.89 (60)	105.53 (70)	103.04 (35)	101.71 (158)	102.49 (147)	107.27 (54)	105.62 (63)	105.23 (78)	106.95 (103)	104.47 (80)	106.84	104.00 (187)	94.69 (160)
Total O =F	101.53 (41)	102.29 (116)	102.41 (53)	103.16 (62)	101.51 (27)	100.97 (157)	102.16 (144)	102.77 (55)	101.61 (49)	102.76 (68)	102.73 (88)	102.79 (74)	102.46	102.06 (188)	93.30 (168)
P	1.01 (0)	1.01 (1)	1.01 (0)	1.02 (1)	1.02 (1)	1.01 (1)	1.02 (1)	1.01 (1)	1.01 (0)	1.01 (0)	1.01 (0)	1.01 (1)	1.01	1.01 (1)	1.02 (1)
Al	0.98 (1)	0.98 (1)	0.98 (0)	0.97 (1)	0.97 (1)	0.99 (1)	0.97 (1)	0.98 (1)	0.98 (1)	0.98 (1)	0.98 (1)	0.99 (1)	0.98	0.98 (2)	0.97 (1)
Na	0.04 (3)	0.07 (4)	tr.	bdl	bdl	bdl	bdl	0.01 (0)	0.01 (0)	0.01 (0)	bdl	tr.	bdl	bdl	bdl
F	0.76 (3)	0.50 (11)	0.81 (1)	0.42 (5)	0.27 (2)	0.14 (1)	0.06 (1)	0.81 (1)	0.73 (4)	0.44 (4)	0.76 (3)	0.30 (4)	0.79	0.35 (4)	0.27 (4)
Li	0.96 (3)	0.93 (4)	1.00 (0)	1.00 (1)	1.00 (0)	1.00 (0)	1.00 (0)	0.99 (0)	0.99 (0)	0.99 (0)	1.00 (0)	0.99 (1)	1.00	1.00 (0)	1.00 (0)
OH	0.24 (3)	0.50 (11)	0.19 (1)	0.58 (5)	0.73 (2)	0.86 (1)	0.94 (1)	0.19 (1)	0.27 (4)	0.56 (4)	0.24 (3)	0.70 (4)	0.21	0.65 (4)	0.73 (4)
Σcat.	2.99 (0)	2.99 (0)	2.99 (0)	2.99 (0)	2.99 (0)	2.99 (1)	2.99 (0)	2.99 (0)	2.99 (0)	2.99 (0)	2.99 (0)	2.99 (0)	2.99	2.99 (1)	2.99 (1)
F/(F+OH)	0.76 (3)	0.50 (11)	0.81 (1)	0.42 (5)	0.27 (2)	0.14 (1)	0.06 (1)	0.81 (1)	0.73 (4)	0.44 (4)	0.76 (3)	0.30 (4)	0.79	0.35 (4)	0.27 (4)

Amblygonite-Montebrasite calculated on 4 oxygens - Hydroxyls calculated by difference on fluorine site (1-F) - Li calculated by difference on lithium site (1-Na)

272   **4.2.   Sodium phosphates**

273

274   Lacroixite [*NaAlPO₄F*] - Lacroixite is present in all samples from all localities as a diffuse

275   alteration of amblygonite-montebrasite occurring as a micron-size mesh and occasionally showing

276   submillimetre whitish veinlets. Observations with cathodoluminescence show 1 or 2 generations of

277   diffuse lacroixite (Fig. 5a) while a secondary euhedral lacroixite grows on vein walls, reaching up to

278   ~100 μm in length and is often associated with fluorapatite. All generations of lacroixite in all

279   deposits tend to have relatively distinctive cathodoluminescent features (Fig. 2b).

280   Lacroixite chemical composition and crystal structure in all deposits show characteristics near

281   the ideal lacroixite (Table 2).
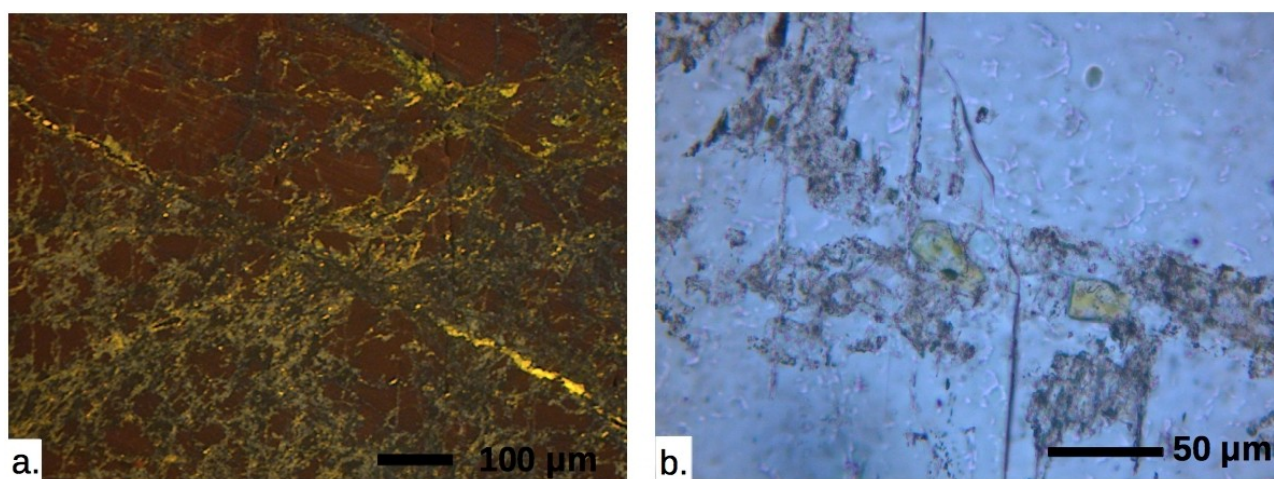
282   Figure 5. a. Primary and secondary amblygonite (brown) with meshy lacroixite (grey-blue) and veinlets (yellow) with a late filling of

283   fluorapatite (bright yellow). Sample BW1. b. Small subhedral yellowish crystals of Mineral C with possibly a natrophilite associated

284   with it. Sample KBB2.

285

286
287
288
289
290
291
292
293
294
295
296
297
298
299
300
301
302
303
304
305
306
307
308
309
310

Table 2. Composition of lacroixite

Sample	KBB2	MONT2-a	MONT2-b	MONT2-c	MONT2-d	MONT2-UCL	MONT2-UCL	MONT3-a	MONT10-a	MONT10-UCL	MONT13-a	MONT20-a
phase		blue CL	yellow CL	cream CL				vein				
n	5	9	3	3	3			6	8	5	2	5
P_2O_5	44.38 (43)	41.30 (14)	40.27 (63)	43.94 (23)	42.91 (148)	42.07 (195)	40.87 (159)	42.25 (179)	43.05 (80)	41.01 (104)	44.06 (93)	44.87 (69)
Al_2O_3	31.21 (31)	31.77 (11)	32.13 (17)	31.22 (33)	31.70 (56)	31.31 (21)	31.04 (45)	31.44 (26)	31.48 (64)	31.49 (14)	31.72 (95)	31.17 (34)
Na_2O	16.95 (48)	18.41 (22)	18.54 (5)	18.03 (14)	18.11 (19)	16.24 (136)	16.57 (206)	17.74 (74)	17.74 (74)	17.51 (51)	15.16 (75)	15.79 (86)
F	11.87 (49)	13.15 (263)	18.24 (74)	12.81 (47)	14.83 (215)	12.71 (257)	13.42 (292)	15.21 (108)	11.35 (43)	13.57 (37)	10.46 (31)	11.63 (53)
Li_2O	0.99 (23)	tr.	bdl	0.46 (9)	0.36 (19)	1.05 (81)	tr.	1.00 (59)	0.51 (35)	0.37 (18)	1.80 (55)	1.56 (45)
Total	105.40 (70)	104.70 (318)	109.18 (36)	106.46 (79)	107.90 (132)	103.37 (119)	102.68 (248)	106.29 (143)	104.14 (296)	103.95 (93)	103.21 (137)	105.02 (103)
Total O =F	100.41 (61)	99.16 (301)	101.50 (43)	101.07 (65)	101.66 (53)	98.02 (55)	97.03 (166)	99.88 (151)	99.36 (282)	98.24 (107)	98.80 (150)	100.12 (95)
P	1.02 (1)	0.97 (0)	0.96 (1)	1.01 (0)	0.99 (2)	1.00 (3)	0.99 (3)	1.00 (2)	1.00 (2)	0.98 (1)	1.02 (0)	1.03 (1)
Al	1.00 (1)	1.04 (0)	1.06 (1)	1.00 (1)	1.02 (3)	1.04 (2)	1.05 (2)	1.04 (2)	1.02 (2)	1.05 (2)	1.03 (1)	1.00 (1)
Na	0.89 (2)	1.00 (1)	1.01 (1)	0.95 (1)	0.96 (2)	0.89 (9)	0.92 (11)	0.89 (6)	0.94 (4)	0.96 (2)	0.81 (5)	0.83 (5)
F	1.02 (4)	1.16 (23)	1.62 (8)	1.10 (4)	1.29 (20)	1.13 (25)	1.22 (28)	1.35 (12)	0.99 (4)	1.21 (5)	0.91 (4)	1.00 (5)
Li	0.11 (2)	tr.	bdl	0.05 (1)	0.04 (2)	0.11 (9)	tr.	0.11 (6)	0.06 (4)	0.04 (2)	0.19 (5)	0.17 (5)
Σcat.	3.02 (1)	3.02 (0)	3.03 (1)	3.01 (0)	3.02 (1)	3.04 (1)	3.04 (2)	3.04 (1)	3.02 (1)	3.03 (1)	3.05 (2)	3.03 (1)
F/(F+OH)	0.99 (1)	1.00 (0)	1.00 (0)	1.00 (0)	1.00 (0)	0.96 (9)	1.00 (1)	1.00 (0)	0.99 (2)	1.00 (0)	0.91 (4)	0.98 (2)

Lacroixite calculated on 9 electrical charges - Hydroxyls calculated by difference on fluorine site (1-F) - Li calculated by difference on sodium site (1-Na)
Sample KBB2, MONT2-a and MOnT10 are corrected for F-content

311   Wardite [*NaAl$_3$(PO$_4$)$_2$(OH)$_4$•2H$_2$O*] - Wardite is observed in Montebras in alteration vugs of

312   quartz veins, containing wavellite, variscite, turquoise and apatite. Apatite replacement is common

313   and it is possible that apatite-rich fine aggregates in other localities are completely altered wardite

314   (Fig. 6a) (Table 3).

315

316   Mineral C [*NaMnFe$_2$(PO$_4$)$_3$*] - In Namibia, at Habis Farm, small subhedral light brown crystals

317   of ~20 μm sparsely disseminated in amblygonite and associated with lacroixite and topaz were

318   found (Fig. 3b). Chemical analysis gives Na$_{0.96}$Ca$_{0.02}$Fe$_{2.16}$Mn$_{0.97}$Mn$_{0.68}$Mg$_{0.01}$Cu$_{0.01}$Al$_{0.04}$(PO$_4$)$_{3.00}$

319   (Table 3) that resembles a heavily oxidised alluaudite similar to some synthetic crystals of Hatert et

320   al. (2006).

Table 3. Composition of various accessory phosphate phases

Sample	KBB2	MONT5	MONT5	MONT5	MONT2	MONT9	MONT12	MONT12	MONT12	MONT12	MONT2	MONT2	MONT5	KBB3
phase	Mineral C	Eosphorite	Eosphorite	Eosphorite	Triplite	Wardite	Morinite	Morinite	Morinite	Morinite	Vitaniemiite	Vitaniemiite	Mineral D	Mineral E
n	4	8	3	3	4	9	6	17	6	15	8	6	8	9
P_2O_5	45.12 (43)	31.41 (52)	31.31 (52)	31.81 (11)	32.23 (64)	36.10 (46)	29.74 (79)	28.27 (141)	28.14 (206)	29.46 (76)	30.28 (118)	27.66 (46)	29.65 (63)	29.19 (66)
SiO_2	bdl	0.04 (2)	0.05 (2)	0.04 (1)	bdl	n.a.	n.a.	n.a.	n.a.	n.a.	n.a.	n.a.	n.a.	n.a.
Al_2O_3	0.43 (46)	21.57 (33)	21.41 (31)	21.95 (23)	0.04 (1)	37.27 (76)	21.15 (58)	21.01 (74)	21.26 (49)	20.59 (51)	21.92 (60)	21.76 (15)	20.16 (17)	20.53 (37)
FeO	18.18 (45)	8.54 (75)	9.88 (113)	8.01 (122)	1.96 (8)	n.a.	n.a.	n.a.	n.a.	n.a.	tr.	tr.	1.30 (36)	0.92 (16)
MnO	24.78 (47)	20.86 (67)	20.49 (150)	21.83 (90)	59.99 (53)	n.a.	n.a.	n.a.	n.a.	n.a.	3.42 (29)	2.25 (42)	14.05 (101)	11.69 (200)
CuO	0.11 (6)	bdl	bdl	0.10 (4)	n.a.	n.a.	n.a.	n.a.	n.a.	n.a.	n.a.	n.a.	n.a.	n.a.
MgO	0.06 (3)	bdl	bdl	bdl	bdl	0.13 (8)	n.a.	n.a.	n.a.	n.a.	2.21 (38)	0.10 (2)	0.08 (4)	tr.
CaO	0.28 (10)	0.40 (9)	0.20 (4)	0.06 (1)	0.71 (1)	0.52 (53)	22.72 (20)	22.33 (52)	22.42 (49)	22.79 (47)	16.89 (129)	21.70 (70)	9.67 (118)	12.21 (190)
SrO	bdl	bdl	bdl	bdl	0.10 (2)	n.a.	n.a.	n.a.	n.a.	n.a.	n.a.	n.a.	n.a.	n.a.
BaO	0.21 (10)	bdl	bdl	bdl	bdl	n.a.	n.a.	n.a.	n.a.	n.a.	n.a.	n.a.	n.a.	n.a.
Na_2O	6.33 (13)	bdl	bdl	0.08 (1)	bdl	7.24 (35)	5.89 (19)	4.96 (27)	3.69 (28)	6.15 (15)	12.90 (28)	11.79 (16)	12.07 (44)	11.51 (49)
F	bdl	0.54 (32)	0.13 (23)	0.12 (14)	8.50 (45)	0.79 (17)	16.74 (99)	16.23 (92)	14.56 (56)	17.19 (99)	17.41 (72)	19.56 (61)	15.33 (62)	14.77 (60)
H_2O	3.82 (4)	16.07 (75)	15.88 (98)	15.31 (17)	bdl	17.56 (71)	10.19 (189)	13.80 (258)	15.89 (327)	10.37 (145)	3.16 (38)	1.66 (20)	3.57 (36)	3.86 (24)
Total	99.31 (98)	99.64 (34)	99.58 (29)	99.44 (11)	103.62 (102)	99.61 (37)	106.44 (56)	106.60 (68)	105.96 (120)	106.56 (58)	108.22 (137)	106.50 (112)	106.04 (127)	105.07 (152)
Total O =F	99.31 (97)	99.41 (26)	99.53 (22)	99.38 (14)	100.04 (100)	99.28 (36)	99.38 (56)	99.77 (53)	99.83 (112)	99.32 (56)	100.89 (121)	98.26 (86)	99.58 (133)	98.85 (135)
P	3.02 (2)	1.02 (1)	1.02 (1)	1.02 (1)	1.02 (1)	2.05 (2)	2.03 (3)	2.00 (4)	2.00 (8)	2.02 (3)	1.01 (2)	0.96 (1)	1.04 (1)	1.02 (1)
Al	0.04 (4)	0.98 (2)	0.97 (2)	0.98 (1)	bdl	2.94 (5)	2.00 (7)	2.06 (6)	2.11 (10)	1.97 (4)	1.02 (1)	1.05 (1)	0.99 (2)	1.00 (2)
Fe	1.20 (3)	0.27 (3)	0.32 (4)	0.25 (4)	0.04 (0)	n.a.	n.a.	n.a.	n.a.	n.a.	tr.	tr.	0.05 (1)	0.03 (1)
Mn	1.66 (3)	0.68 (2)	0.67 (4)	0.70 (3)	1.90 (2)	n.a.	n.a.	n.a.	n.a.	n.a.	0.11 (1)	0.08 (2)	0.49 (3)	0.41 (8)
Cu	0.01 (0)	bdl	bdl	bdl	n.a.	n.a.	n.a.	n.a.	n.a.	n.a.	n.a.	n.a.	n.a.	n.a.
Mg	0.01 (0)	bdl	bdl	bdl	bdl	0.01 (1)	n.a.	n.a.	n.a.	n.a.	0.13 (2)	0.01 (0)	0.01 (0)	tr.
Ca	0.02 (1)	0.02 (0)	0.01 (0)	bdl	0.03 (0)	0.04 (4)	1.96 (2)	1.99 (4)	2.02 (5)	1.98 (4)	0.71 (6)	0.96 (3)	0.43 (5)	0.54 (8)
Sr	bdl	bdl	bdl	bdl	bdl	n.a.	n.a.	n.a.	n.a.	n.a.	n.a.	n.a.	n.a.	n.a.
Ba	0.01 (0)	bdl	bdl	bdl	bdl	n.a.	n.a.	n.a.	n.a.	n.a.	n.a.	n.a.	n.a.	n.a.
Na	0.97 (1)	bdl	bdl	0.01 (0)	bdl	0.94 (5)	0.91 (2)	0.80 (3)	0.60 (5)	0.97 (2)	0.98 (1)	0.94 (1)	0.97 (3)	0.92 (3)
F	bdl	0.07 (4)	0.02 (3)	0.01 (2)	1.00 (5)	0.17 (4)	3.97 (15)	4.00 (8)	3.79 (11)	4.19 (12)	2.17 (9)	2.54 (6)	2.01 (9)	1.94 (7)
OH	bdl	1.93 (4)	1.98 (3)	1.99 (2)	0.02 (2)	3.83 (4)	1.03 (15)	1.00 (8)	1.21 (11)	0.81 (12)	0.83 (9)	0.46 (6)	0.99 (9)	1.06 (7)
H_2O	2.02 (2)	1.10 (11)	1.05 (16)	0.95 (4)	bdl	2.01 (19)	2.41 (42)	3.45 (94)	3.93 (118)	2.49 (40)				
Σcat.	6.94 (4)	2.99 (1)	3.00 (0)	2.98 (0)	2.99 (0)	5.99 (3)	6.92 (2)	6.88 (5)	6.75 (7)	6.98 (4)	3.98 (4)	4.00 (2)	3.98 (2)	3.95 (2)

322   **4.3.   Sodium-Calcium phosphates**

323

324   Morinite [$NaCa_2Al_2(PO_4)_2(F,OH)_5 \cdot 2H_2O$] - Montebras is the type locality of morinite (Lacroix,

325   1891). It occurs as purple-red masses and fibrous crusts with concentric colour changes filing vugs

326   in late quartz veins. Minerals associated with morinite are crandallite, turquoise and a replacement

327   by apatite (Fig. 6b). Like wardite, a common replacement product of morinite is a fibrous sodium-

328   rich apatite indicating that other localities could host completely replaced morinite although no such

329   apatite has been observed in our morinite-free localities (Table 3).
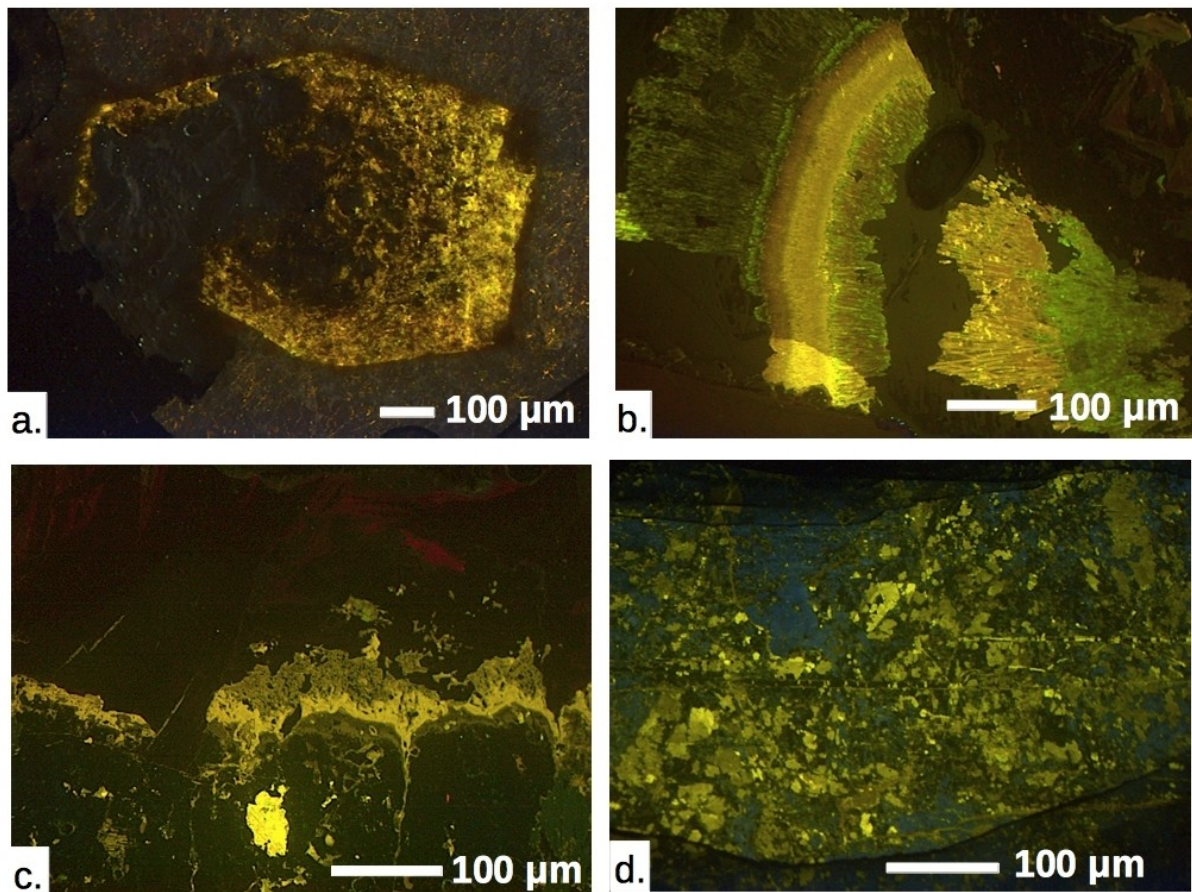
331   Figure 6. a. Sodium-rich apatite pseudomorph of an euhedral wardite crystal in a quartz vein in CL-PPL. (Sample MONT3). b.

332   Fibrous sodium-rich apatite pseudomorph of a morinite crust preserving some of the original zonation in CL-PPL (Sample

333   MONT12). c. Amblygonite (dark) and a large pocket of lacroixite (dark blue) with a fluorapatite (yellow) reaction zone in contact

334   with polylithionite (dark red) in CL-PPL (Sample KBB2). d. Fluorapatite (yellow) replacement of primary amblygonite (blue-grey) in

335   CL-PPL (Sample KBB2).

336   Viitaniemiite-like minerals [*Na(Ca,Mn,Fe)Al(PO$_4$)(F,OH)$_3$*] - Viitaniemiite is a rare mineral that

337   occurs in Montebras as a colourless phase in altered amblygonite. It is pervasively mixed with

338   lacroixite as rare patches of a couple of hundred microns. Viitaniemiite is identifiable in

339   cathodoluminescence with a brown-orange colour of medium intensity (Fig. 7).

340   The simplified composition of Montebras viitaniemiite is $Na_{0.9}(Ca_{0.8}Mn_{0.1}Mg_{0.1})Al(PO_4)$

341    $(F_{2.3}OH_{0.7})$. However, another Mn-rich viitaniemiite-like mineral is observed in Montebras as a

342   likely alteration product of eosphorite. Grains are up to 250 μm and have an ideal composition

343    $Na(Mn,Ca)Al(PO_4)(F,OH)_3$. Finally, in McDonalds pegmatite, a Fe-rich viitaniemiite-like mineral is

344   observed with a composition $Na_{0.91}(Ca_{0.59}Fe_{0.34}Mg_{0.05}Mn_{0.02})Al_{0.97}(PO_4)_{1.03}(F_{2.09}OH_{0.64})$ (Table 3) (Fig.

345   8).

346   Figure 7. View of an assemblage of primary amblygonite, apatite, corundum and Fe-rich viitaniemiite-like mineral in plane polarised

347   light (a), crossed polars (b) and cathodoluminescence (c) where amblygonite appears dark red, fluorapatite as yellow orange,

348   viitaniemiite-like phase as orange and corundum does not show a strong luminescence. (Sample KBB3).
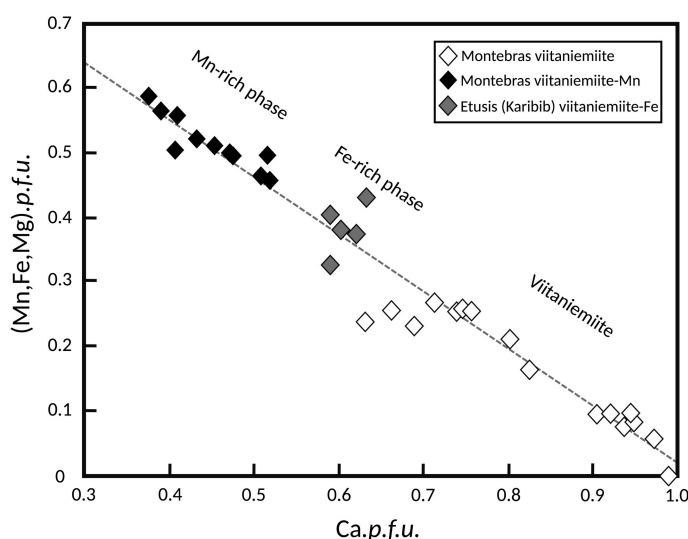
357   Figure 8. Distribution of viitaniemiite-like minerals illustrating the substitution Ca <=> Mn+Fe+Mg.

Table 3. Composition of various accessory phosphate phases

Sample	KBB2	MONT5	MONT5	MONT5	MONT2	MONT9	MONT12	MONT12	MONT12	MONT12	MONT2	MONT2	MONT5	KBB3
phase	Mineral C	Eosphorite	Eosphorite	Eosphorite	Triplite	Wardite	Morinite	Morinite	Morinite	Morinite	Vitaniemiite	Vitaniemiite	Mineral D	Mineral E
n	4	8	3	3	4	9	6	17	6	15	8	6	8	9
P_2O_5	45.12 (43)	31.41 (52)	31.31 (52)	31.81 (11)	32.23 (64)	36.10 (46)	28.14 (206)	28.27 (141)	29.74 (79)	29.46 (76)	30.28 (118)	27.66 (46)	29.65 (63)	29.19 (66)
SiO_2	bdl	0.04 (2)	0.05 (2)	0.04 (1)	bdl	n.a.	n.a.	n.a.	n.a.	n.a.	n.a.	n.a.	n.a.	n.a.
Al_2O_3	0.43 (46)	21.57 (33)	21.41 (31)	21.95 (23)	0.04 (1)	37.27 (76)	21.26 (49)	21.01 (74)	21.15 (58)	20.59 (60)	21.92 (60)	21.76 (15)	20.16 (17)	20.53 (37)
FeO	18.18 (45)	8.54 (75)	9.88 (113)	8.01 (122)	1.96 (8)	n.a.	n.a.	n.a.	n.a.	n.a.	tr.	tr.	1.30 (36)	0.92 (16)
MnO	24.78 (47)	20.86 (67)	20.49 (150)	21.83 (90)	59.99 (53)	n.a.	n.a.	n.a.	n.a.	n.a.	3.42 (29)	2.25 (42)	14.05 (101)	11.69 (200)
CuO	0.11 (6)	bdl	bdl	0.10 (4)	n.a.	n.a.	n.a.	n.a.	n.a.	n.a.	n.a.	n.a.	n.a.	n.a.
MgO	0.06 (3)	bdl	bdl	bdl	bdl	0.13 (8)	n.a.	n.a.	n.a.	n.a.	2.21 (38)	0.10 (2)	0.08 (4)	tr.
CaO	0.28 (10)	0.40 (9)	0.20 (4)	0.06 (1)	0.71 (1)	0.52 (53)	22.42 (49)	22.33 (52)	22.72 (20)	22.79 (70)	16.89 (129)	21.70 (70)	9.67 (118)	12.21 (190)
SrO	bdl	bdl	bdl	bdl	0.10 (2)	n.a.	n.a.	n.a.	n.a.	n.a.	n.a.	n.a.	n.a.	n.a.
BaO	0.21 (10)	bdl	bdl	bdl	bdl	n.a.	n.a.	n.a.	n.a.	n.a.	n.a.	n.a.	n.a.	n.a.
Na_2O	6.33 (13)	bdl	bdl	0.08 (1)	bdl	7.24 (35)	3.69 (28)	4.96 (27)	5.89 (19)	6.15 (15)	12.90 (28)	11.79 (16)	12.07 (44)	11.51 (49)
F	bdl	0.54 (32)	0.13 (23)	0.12 (14)	8.50 (45)	0.79 (17)	14.56 (56)	16.23 (92)	16.74 (160)	17.19 (99)	17.41 (72)	19.56 (61)	15.33 (62)	14.77 (60)
$H2O$	3.82 (4)	16.07 (75)	15.88 (98)	15.31 (17)	bdl	17.56 (71)	15.89 (327)	13.80 (258)	10.19 (189)	10.37 (145)	3.16 (38)	1.66 (20)	3.57 (36)	3.86 (24)
Total	99.31 (98)	99.64 (34)	99.58 (29)	99.44 (11)	103.62 (102)	99.61 (37)	105.96 (120)	106.60 (68)	106.44 (56)	106.56 (58)	108.22 (137)	106.50 (112)	106.04 (127)	105.07 (152)
Total O =F	99.31 (97)	99.41 (26)	99.53 (22)	99.38 (14)	100.04 (100)	99.28 (36)	99.83 (112)	99.77 (53)	99.38 (47)	99.32 (56)	100.89 (121)	98.26 (86)	99.58 (133)	98.85 (135)
P	3.02 (2)	1.02 (1)	1.02 (1)	1.02 (1)	1.02 (1)	2.05 (2)	2.00 (8)	2.00 (4)	2.03 (3)	2.02 (3)	1.01 (2)	0.96 (1)	1.04 (1)	1.02 (1)
Al	0.04 (4)	0.98 (2)	0.97 (2)	0.98 (1)	bdl	2.94 (5)	2.11 (10)	2.06 (6)	2.00 (7)	1.97 (4)	1.02 (1)	1.05 (1)	0.99 (2)	1.00 (2)
Fe	1.20 (3)	0.27 (3)	0.32 (4)	0.25 (4)	0.04 (0)	n.a.	n.a.	n.a.	n.a.	n.a.	tr.	tr.	0.05 (1)	0.03 (1)
Mn	1.66 (3)	0.68 (2)	0.67 (4)	0.70 (3)	1.90 (2)	n.a.	n.a.	n.a.	n.a.	n.a.	0.11 (1)	0.08 (2)	0.49 (3)	0.41 (8)
Cu	0.01 (0)	bdl	bdl	bdl	n.a.	n.a.	n.a.	n.a.	n.a.	n.a.	n.a.	n.a.	n.a.	n.a.
Mg	0.01 (0)	bdl	bdl	bdl	bdl	0.01 (1)	n.a.	n.a.	n.a.	n.a.	0.13 (2)	0.01 (0)	0.01 (0)	tr.
Ca	0.02 (1)	0.02 (0)	0.01 (0)	bdl	0.03 (0)	0.04 (4)	2.02 (5)	1.99 (4)	1.96 (2)	1.98 (4)	0.71 (6)	0.96 (3)	0.43 (5)	0.54 (8)
Sr	bdl	bdl	bdl	bdl	bdl	n.a.	n.a.	n.a.	n.a.	n.a.	n.a.	n.a.	n.a.	n.a.
Ba	0.01 (0)	bdl	bdl	bdl	bdl	n.a.	n.a.	n.a.	n.a.	n.a.	n.a.	n.a.	n.a.	n.a.
Na	0.97 (1)	bdl	bdl	0.01 (0)	bdl	0.94 (5)	0.60 (5)	0.80 (3)	0.91 (2)	0.97 (2)	0.98 (1)	0.94 (1)	0.97 (3)	0.92 (3)
F	bdl	0.07 (4)	0.02 (3)	0.01 (2)	1.00 (5)	0.17 (4)	3.79 (11)	4.00 (8)	3.97 (15)	4.19 (12)	2.17 (9)	2.54 (6)	2.01 (9)	1.94 (7)
OH	2.02 (2)	1.93 (4)	1.98 (3)	1.99 (2)	0.02 (2)	3.83 (4)	1.21 (11)	1.00 (8)	1.03 (15)	0.81 (12)	2.17 (9)	2.54 (6)	2.01 (9)	1.94 (7)
$H2O$		1.10 (11)	1.05 (16)	0.95 (4)		2.01 (19)	3.93 (118)	3.45 (94)	2.41 (42)	2.49 (40)	0.83 (9)	0.46 (6)	0.99 (9)	1.06 (7)
Σcat.	6.94 (4)	2.99 (1)	3.00 (0)	2.98 (0)	2.99 (0)	5.99 (3)	6.75 (7)	6.88 (5)	6.92 (2)	6.98 (4)	3.98 (4)	4.00 (2)	3.98 (2)	3.95 (2)

4.4. Calcium phosphates

Apatite [$Ca_5(PO_4)_3F$] – Apatite is a frequent mineral that form at all stages of crystallisation and hydrothermal alteration, as euhedral crystals, veins (with quartz and lacroixite), radiating masses or microscopic inclusions in montebrasite, crandallite, cassiterite, wavellite and turquoise (Fig. 6).

All apatites in all localities are F-rich end members. Manganese content ranges from 0.2 to 3 wt. % MnO while iron rarely reaches 0.4 wt.% FeO. Apatite associated with morinite and wardite have up to 1 wt.% Na_2O and 0.5 wt.% Al_2O_3 (Table 4).

Abuite [*$CaAl_2(PO_4)_2F_2$*] - The assemblage of amblygonite and 'gormanite' in McDonalds pegmatite contains anhedral patches of a few hundred microns of colourless material that display slightly higher relief than amblygonite and a perfect cleavage plane (Fig. 9). Microprobe analyses give a composition $Ca_{0.99}Na_{0.01}Al_{1.98}(PO_4)_{2.02}F_{2.02}$ (Table 5) which is likely to be abuite, a mineral described in metamorphosed pyroclastics of Hinomaru-Nago mine, Japan (Enju & Uehara, 2015). To our knowledge, McDonalds pegmatite on Etusis farm, Namibia would be the second occurrence of this mineral species.

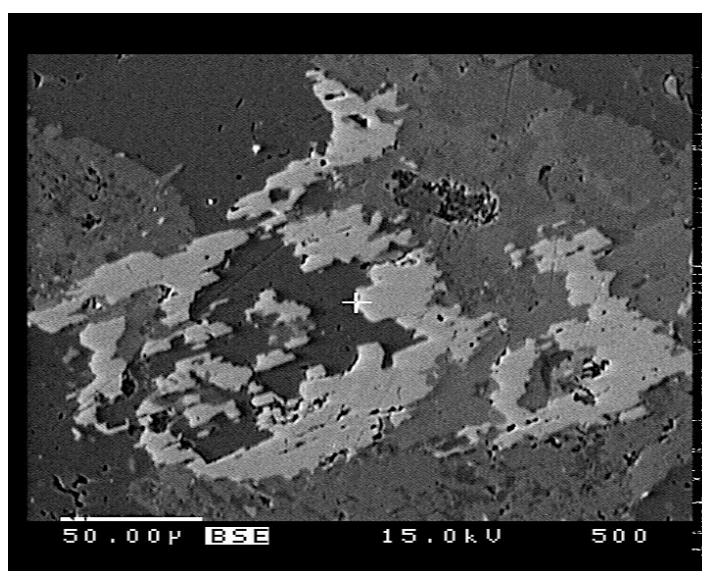Figure 9. Abuite (white) in amblygonite (light grey) altered in variscite (medium grey) and quartz (dark grey) with corundum prisms (altered rectangles) seen in BSE. (Sample KBB3).

Table 4. Composition of apatite

Sample	BW3 orange CL	BW3 green CL	KBB1	KBB2 F-correction	KBB3 F-correction	MONT9	MONT9 brown CL	MONT9	MONT9	MONT12	MONT12	MONT12
phase n	5	3	5	12	6	9	5	3	2	4	10	8
P_2O_5	41.31 (101)	41.02 (69)	41.41 (88)	41.70 (95)	43.12 (44)	41.96 (111)	41.88 (89)	41.49 (130)	43.39 (24)	42.14 (54)	40.18 (83)	40.78 (77)
Al_2O_3	bdl	0.14 (9)	tr.	tr.	bdl	tr.	0.13 (10)	tr.	bdl	0.11 (5)	0.17 (11)	0.22 (15)
FeO	tr.	0.33 (7)	bdl	tr.	0.17 (10)	0.34 (27)	0.33 (10)	0.36 (0)	tr.	0.10 (8)	tr.	tr.
MnO	0.69 (23)	0.16 (15)	bdl	0.36 (24)	1.17 (17)	2.99 (64)	1.24 (36)	1.93 (25)	0.77 (8)	1.04 (54)	0.43 (45)	0.44 (35)
CuO	bdl	tr.	bdl	0.04 (2)	bdl	bdl	bdl	bdl	bdl	0.17 (11)	bdl	bdl
CaO	53.70 (60)	53.82 (28)	55.65 (12)	54.97 (112)	54.04 (48)	51.58 (120)	53.44 (130)	52.39 (62)	53.13 (67)	52.84 (48)	53.80 (104)	53.49 (122)
SrO	bdl	tr.	0.25 (17)	tr.	0.68 (54)	bdl	bdl	bdl	bdl			0.01 (3)
Na_2O	bdl	bdl	0.05 (4)	bdl	bdl	bdl	bdl	bdl	bdl	0.19 (11)	0.41 (35)	tr.
F	4.76 (58)	5.02 (32)	6.08 (32)	3.98 (9)	4.22 (18)	3.56 (30)	4.26 (38)	2.52 (60)	4.64 (20)	4.61 (26)	4.06 (24)	4.33 (77)
H2O												
Total	100.53 (61)	100.56 (46)	103.62 (90)	101.03 (171)	102.57 (42)	100.47 (135)	101.12 (89)	98.71 (78)	102.07 (99)	101.19 (62)	99.07 (147)	99.42 (166)
Total O =F	98.53 (66)	98.44 (59)	101.06 (88)	99.35 (168)	100.80 (34)	98.97 (138)	99.32 (95)	97.65 (103)	100.12 (91)	99.25 (58)	97.37 (148)	97.60 (137)
P	3.00 (4)	2.99 (2)	2.97 (3)	2.99 (2)	3.03 (3)	3.03 (5)	3.00 (3)	3.01 (4)	3.07 (1)	3.03 (2)	3.00 (4)	2.98 (3)
Al	bdl	tr.	tr.	tr.	bdl	tr.	0.02 (1)	tr.	tr.	tr.	tr.	0.02 (1)
Fe	bdl	0.02 (0)	bdl	bdl	tr.	tr.	bdl	tr.	bdl	tr.	bdl	bdl
Mn	0.05 (2)	tr.	bdl	0.03 (2)	0.08 (1)	0.22 (5)	0.09 (2)	0.14 (2)	0.05 (1)	0.07 (4)	0.04 (2)	tr.
Cu	tr.	tr.	bdl	bdl	bdl	bdl	bdl	bdl	bdl	bdl	0.01 (0)	bdl
Ca	4.94 (10)	4.97 (6)	5.06 (6)	4.99 (7)	4.80 (4)	4.71 (10)	4.89 (8)	4.82 (11)	4.76 (2)	4.81 (5)	4.96 (11)	5.03 (8)
Sr	bdl	bdl	tr.	tr.	tr.	tr.						
Na	bdl	tr.	tr.	tr.	bdl	tr.	tr.	0.01 (0)	0.01 (0)	0.05 (2)	0.07 (4)	0.13 (3)
F	1.18 (5)	1.37 (10)	1.63 (9)	1.02 (430)	1.11 (5)	0.96 (8)	1.03 (2)	0.69 (18)	1.23 (4)	1.24 (7)	1.11 (9)	1.12 (7)
OH	bdl	bdl	bdl	bdl	bdl	0.06 (6)	bdl	0.31 (18)	0.17 (468)			
Σcat.	3.01 (47)	3.02 (84)	8.07 (4)	8.06 (9)	7.96 (4)	8.00 (6)	8.02 (2)	8.02 (8)	3.03 (101)	8.02 (5)	8.10 (4)	8.19 (4)
F/(F+OH)	1.00	1.00	1.00	1.00	1.00	0.96	1.00	0.69	1.00	0.96	1.00	1.00

Apatite calculated on 25 electrical charges - Hydroxyls calculated by difference on fluorine site (1-F)

386

Table 5. Composition of abuite

Sample phase	KBB3	KBB3	KBB3
n	4	7	6
P_2O_5	45.58 (72)	44.19 (51)	44.61 (62)
Al_2O_3	31.56 (17)	31.72 (17)	31.48 (12)
CaO	17.17 (13)	17.18 (24)	17.49 (12)
SrO	*bdl*	*bdl*	0.21 (9)
Na_2O	*bdl*	0.08 (5)	0.17 (12)
F	12.20 (5)	12.38 (7)	11.46 (36)
H_2O			0.20 (18)
Total	106.78 (68)	105.72 (36)	105.65 (42)
Total O =F	101.64 (69)	100.51 (36)	100.82 (51)
P	2.03 (1)	2.00 (2)	2.01 (1)
Al	1.96 (2)	2.00 (2)	1.98 (2)
Ca	0.97 (1)	0.99 (2)	1.00 (1)
Sr	*bdl*	*bdl*	0.01 (0)
Na	*bdl*	0.01 (1)	0.02 (1)
F	2.04 (3)	2.10 (2)	1.93 (7)
OH	0.00	0.00	0.07 (6)
Σcat.	4.98 (1)	5.01 (1)	5.02 (2)
F/(F+OH)	1.00	1.00	0.96 (3)

Abuite calculated on 18 electrical charges
Hydroxyls calculated by difference on fluorine site (2-F)
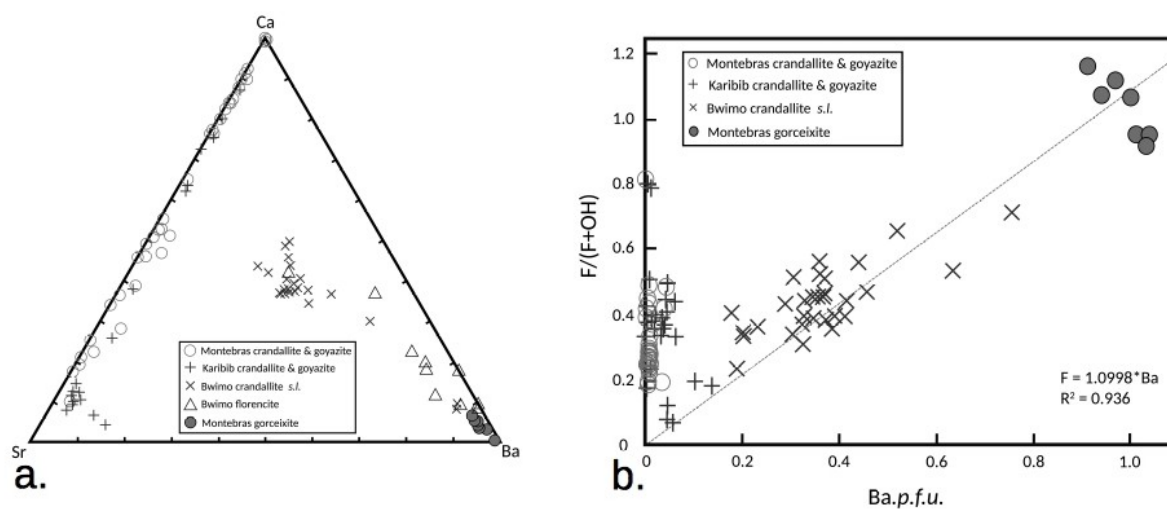
399 *Figure 10. a. Distribution of crandallite group mineral as a proportion of Ca, Sr and Ba in the three localities. A complete solid*

400 *solution between crandallite and goyazite exists in Montebras and Karibib while gorceixite contain little Ca-Sr. Bwimo crandallite*

401 *group minerals are intermediary between Ca-Sr and Ba and also show Ba-rich florencites. b. Correlation between Ba content in*

402 *crandallite and fluorine substitution on the hydroxyl site. The correlation only appears for crandallite group minerals that contains*

403 *>0.1 Ba.p.f.u..*

404

405   Crandallite group [$(Ca,Sr,Ba)Al_3(PO_4)(PO_3OH)(OH)_6 \bullet H_2O$ - $(REE)Al_3(PO_4)_2(OH)_6$] –

406   Crandallite *s.l.* are common in all localities and show extensive substitution in the Ca-Sr-Ba-REE

407   space (Fig. 10). Barium-poor crandallite and goyazite are very common and occur as veinlets

408   associated with most other phosphates in Montebras and Karibib. In Montebras' morinite, Ba-free

409   crandallite-goyazite crystallised as zoned euhedral rhombohedra (Pirard, 2022). Gorceixite in

410   Montebras forms thick crusts on kaolinite and has a chemical composition near the Ba end-member.

411   In Bwimo, deeply altered facies of kaolinite and wavellite are incrusted with gorceixite, florencite

412   and rarer goyazite-crandallite grains (Table 6, Fig. 10).

413

414

Table 6. Composition of crandallite group

Sample phase	MONT7	MONT7	MONT9	MONT12	MONT12	MONT12	MONT12	MONT12	MONT12
n	5	3	3	5	7	3	4	5	2
P_2O_5	25.78 (26)	26.33 (49)	32.55 (98)	29.40 (43)	27.76 (143)	27.40 (327)	29.22 (284)	23.48 (102)	26.77 (85)
Al_2O_3	27.73 (15)	27.38 (30)	32.65 (77)	34.06 (33)	35.56 (61)	32.42 (111)	37.54 (444)	31.96 (129)	33.22 (45)
FeO	0.59 (21)	0.85 (66)	bdl	bdl	bdl	bdl	bdl	bdl	0.04 (1)
MnO	bdl	bdl	bdl	bdl	bdl	0.13 (12)	bdl	bdl	bdl
CuO	0.17 (4)	0.08 (4)	bdl	0.13 (5)	bdl	0.06 (3)	bdl	0.07 (3)	0.14 (11)
CaO	0.58 (9)	0.26 (19)	5.64 (77)	6.58 (42)	11.04 (45)	3.37 (196)	12.90 (101)	2.68 (48)	5.58 (30)
SrO	0.52 (3)	0.32 (22)	11.57 (159)	10.99 (53)	3.34 (168)	15.98 (145)	0.63 (126)	18.10 (32)	12.00 (99)
BaO	26.72 (91)	28.68 (25)	1.31 (26)	0.28 (18)	bdl	bdl	bdl	0.19 (24)	bdl
Na_2O	0.07 (2)	0.09 (3)	bdl	0.04 (3)	bdl	0.01 (0)	bdl	bdl	0.03 (1)
K_2O	0.22 (5)	0.11 (8)	bdl	bdl	bdl	bdl	bdl	bdl	bdl
F	3.83 (14)	3.24 (5)	1.56 (68)	1.15 (4)	1.14 (37)	2.34 (219)	1.09 (12)	1.34 (27)	1.30 (25)
H_2O	15.51 (53)	13.74 (124)	14.13 (82)	18.89 (85)	23.79 (300)	20.11 (571)	21.46 (732)	25.74 (162)	23.14 (162)
Total	102.17 (22)	101.71 (32)	99.77 (83)	101.67 (17)	103.00 (55)	102.46 (125)	103.05 (46)	103.78 (77)	102.56 (45)
Total O =F	100.55 (25)	100.35 (33)	99.11 (64)	101.19 (18)	102.52 (68)	101.47 (203)	102.60 (41)	103.21 (73)	102.02 (35)
P	1.99 (2)	2.02 (1)	2.07 (5)	1.92 (1)	1.82 (5)	1.89 (16)	1.82 (1)	1.74 (6)	1.85 (3)
Al	2.98 (2)	2.93 (4)	2.89 (8)	3.10 (4)	3.25 (11)	3.13 (19)	3.26 (6)	3.31 (12)	3.20 (9)
Fe	0.05 (2)	0.06 (5)	bdl	bdl	bdl	bdl	bdl	bdl	0.00 (0)
Mn	bdl	bdl	bdl	bdl	bdl	0.01 (1)	bdl	bdl	bdl
Cu	0.02 (1)	bdl	bdl	bdl	bdl	0.01 (0)	bdl	0.01 (0)	0.02 (1)
Ca	0.06 (1)	0.03 (2)	0.45 (6)	0.54 (3)	0.92 (3)	0.30 (18)	1.02 (2)	0.25 (4)	0.49 (2)
Sr	0.03 (0)	0.02 (1)	0.50 (7)	0.49 (3)	0.15 (7)	0.76 (5)	0.03 (6)	0.92 (2)	0.57 (4)
Ba	0.96 (3)	1.02 (1)	0.04 (1)	bdl	bdl	bdl	bdl	bdl	0.01 (1)
Na	0.01 (0)	0.02 (1)	bdl	0.01 (0)	bdl	bdl	bdl	bdl	0.01 (0)
K	0.03 (1)	bdl	bdl	bdl	bdl	bdl	bdl	bdl	bdl
F	1.11 (4)	0.93 (2)	0.37 (16)	0.28 (1)	0.28 (8)	0.59 (53)	0.25 (1)	0.37 (8)	0.34 (7)
OH	3.89 (4)	4.07 (2)	4.63 (16)	4.72 (1)	4.72 (8)	4.41 (53)	4.75 (1)	4.63 (8)	4.66 (7)
H_2O	2.78 (18)	2.12 (41)	1.23 (27)	2.51 (25)	3.81 (87)	3.32 (147)	3.07 (217)	5.23 (62)	3.98 (56)
Σ(Ca,Sr,Ba)	1.04 (3)	1.06 (4)	1.00 (1)	1.05 (3)	1.07 (8)	1.07 (14)	1.05 (7)	1.18 (5)	1.07 (5)
F/(F+OH)	0.22 (1)	0.19 (0)	0.07 (3)	0.06 (0)	0.06 (2)	0.12 (11)	0.05 (0)	0.07 (2)	0.07 (1)

Crandallite group calculated on 21 electrical charges - Hydroxyls calculated by difference on fluorine site (5-F)
H2O calculated by difference on total measured and calculated hydroxyl groups

415   **4.5.**   **Cation-free aluminium phosphates**

416

417   Variscite [*AlPO$_4$•2H$_2$O*] - Variscite is a common cryptocrystalline cream-coloured phase

418   forming an intimate mixture with kaolinite, wavellite and quartz on the outer part of most samples

419   of Montebras and Bwimo. In Bwimo, variscite sometimes occurs as thicker veins cross-cutting

420   altered masses of amblygonite-montebrasite.

421

422   Wavellite [*Al$_3$(PO$_4$)$_2$(OH,F)$_3$•5H$_2$O*] – Wavellite forms characteristic acicular aggregates, crusts

423   and independent needles up to 5 mm. In Montebras, wavellite is associated with many alteration

424   phases and rarely in direct contact with amblygonite. In Bwimo, residual masses of montebrasite

425   remain in wavellite. .

Table 7. Composition of wavellite, variscite and turquoise

Sample	BW1	BW1	BW5	BW8	BW7	MONT13	MONT15	BW1	BW3	BW5	BW7	BW8	BW1	MONT5 vein	MONT3
phase n	7	2	4	3	4	2	2	5	6	4	3	4	8	3	2
P_2O_5	35.38 (72)	39.51 (65)	34.27 (87)	35.02 (21)	35.12 (43)	34.88 (72)	34.58 (67)	50.51 (83)	44.50 (65)	45.53 (171)	45.55 (20)	44.91 (77)	34.31 (114)	33.65 (205)	33.70 (94)
Al_2O_3	36.31 (54)	38.71 (63)	35.30 (35)	36.32 (50)	36.92 (66)	35.66 (60)	35.56 (22)	35.37 (27)	31.53 (19)	32.15 (62)	32.88 (70)	31.94 (84)	36.44 (37)	34.66 (140)	34.97 (141)
FeO	bdl	0.05 (3)	0.06 (3)	bdl	bdl	0.10 (3)	0.08 (6)	0.04 (3)	bdl	0.04 (3)	0.16 (12)	0.06 (2)	bdl	0.09 (7)	2.16 (44)
MnO	bdl	bdl	bdl	bdl	0.07 (3)	bdl	0.11 (3)	bdl	bdl	bdl	0.02 (1)	bdl	n.a	n.a	n.a
CuO	bdl	0.04 (1)	bdl	bdl	bdl	bdl	0.08 (7)	bdl	bdl	bdl	bdl	bdl	8.36 (42)	4.36 (259)	5.26 (77)
CaO	bdl	bdl	0.05 (2)	bdl	0.03 (2)	0.03 (1)	bdl	bdl	bdl	0.05 (2)	0.03 (2)	bdl	0.11 (6)	0.62 (51)	1.21 (83)
Na_2O	bdl	0.01 (0)	bdl	bdl	bdl	bdl	bdl	bdl	bdl	bdl	bdl	bdl	bdl	bdl	0.57 (48)
K_2O	0.06 (2)	0.05 (2)	0.09 (3)	0.03 (2)	0.10 (2)	0.07 (4)	0.15 (3)	bdl	0.04 (3)	bdl	0.02 (1)	bdl	0.13 (3)	0.16 (3)	0.12 (2)
F	4.25 (17)	4.22 (3)	3.80 (10)	4.08 (7)	3.92 (10)	3.96 (4)	4.00 (22)	2.48 (60)	0.18 (3)	0.20 (7)	0.13 (12)	0.16 (9)	0.94 (22)	1.11 (28)	2.23 (22)
H_2O	24.96 (95)	17.59 (132)	27.35 (138)	25.48 (51)	25.09 (34)	26.05 (71)	26.47 (117)	10.99 (66)	23.36 (84)	21.65 (266)	21.19 (23)	22.60 (65)	19.48 (175)	23.78 (471)	20.25 (23)
Total	101.12 (44)	100.31 (5)	101.02 (32)	101.24 (26)	101.34 (42)	100.98 (56)	101.14 (12)	99.63 (38)	99.86 (26)	99.80 (31)	100.19 (36)	99.94 (67)	100.11 (55)	99.51 (130)	100.63 (102)
Total O =F	99.33 (41)	98.53 (6)	99.42 (32)	99.52 (24)	99.69 (43)	99.32 (54)	99.46 (21)	98.59 (28)	99.78 (26)	99.72 (34)	100.14 (40)	99.87 (67)	99.72 (55)	99.04 (121)	99.69 (112)
P	2.05 (3)	2.09 (0)	2.04 (2)	2.04 (1)	2.02 (3)	2.05 (4)	2.04 (1)	1.01 (1)	1.01 (1)	1.01 (1)	1.00 (1)	1.00 (2)	4.05 (7)	4.17 (17)	4.07 (13)
Al	2.92 (4)	2.85 (0)	2.93 (3)	2.94 (2)	2.96 (5)	2.92 (6)	2.93 (2)	0.98 (1)	0.99 (1)	0.99 (1)	1.00 (2)	0.99 (3)	5.98 (12)	5.99 (21)	5.88 (21)
Fe	bdl	bdl	bdl	bdl	bdl	0.01 (0)	bdl	bdl	bdl	bdl	tr.	tr.	bdl	bdl	0.26 (5)
Mn	bdl	bdl	bdl	bdl	bdl	bdl	0.01 (0)	bdl	bdl	tr.	tr.	bdl	n.a	n.a	n.a
Cu	bdl	bdl	bdl	bdl	bdl	bdl	bdl	bdl	bdl	tr.	bdl	bdl	0.88 (4)	0.47 (26)	0.57 (8)
Ca	bdl	bdl	bdl	bdl	bdl	bdl	bdl	bdl	bdl	bdl	bdl	bdl	0.02 (1)	0.10 (8)	0.19 (13)
Na	bdl	bdl	bdl	bdl	bdl	bdl	bdl	bdl	bdl	bdl	bdl	bdl	bdl	bdl	0.16 (13)
K	bdl	bdl	0.01 (0)	bdl	0.01 (0)	0.01 (0)	0.01 (0)	bdl	bdl	bdl	tr.	bdl	0.02 (1)	0.03 (1)	0.02 (0)
F	0.92 (4)	0.83 (1)	0.85 (2)	0.89 (2)	0.84 (2)	0.87 (1)	0.88 (4)	0.19 (5)	0.01 (0)	0.02 (1)	tr.	tr.	0.41 (10)	0.52 (15)	1.01 (10)
OH	2.08 (4)	2.17 (1)	2.15 (2)	2.11 (2)	2.16 (2)	2.13 (1)	2.12 (4)	n.a	n.a	n.a	n.a	n.a	7.59 (10)	7.48 (15)	6.99 (10)
H_2O	4.65 (29)	2.59 (34)	5.36 (44)	4.78 (16)	4.62 (10)	4.97 (19)	5.11 (34)	0.87 (6)	2.08 (9)	1.89 (29)	1.83 (2)	1.99 (6)	5.27 (96)	7.98 (291)	6.14 (20)
Σcat.	4.98 (2)	4.96 (0)	4.99 (2)	5.00 (2)	5.00 (2)	4.99 (2)	5.01 (2)	2.00 (1)	2.00 (1)	2.00 (1)	2.01 (0)	2.01 (1)	10.97 (6)	10.81 (23)	11.13 (22)
F/(F+OH)	0.31 (1)	0.28 (0)	0.28 (1)	0.30 (1)	0.28 (1)	0.29 (0)	0.29 (1)	n.a	n.a	n.a	n.a	n.a	0.05 (1)	0.06 (2)	0.13 (1)

Wavellite calculated on 19 electrical charges - Hydroxyls calculated by difference on hydroxyl site (3-F)
H2O calculated by difference on total measured and calculated hydroxyls groups
Variscite calculated on 8 electrical charges - H2O calculated by difference on total measured
Turquoise calculated on 40 electrical charges - Hydroxyls calculated by difference on hydroxyl site (8-F)
H2O calculated by difference on total measured and calculated hydroxyl groups

427   **4.6.   Transition metal phosphates**

428

429   Turquoise [$CuAl_6(PO_4)_4(OH)_8•4H_2O$] - Turquoise is a very common mineral in Montebras and

430   subordinate in Bwimo, giving bluish to greenish tints to altered masses of phosphate. Textures vary

431   from massive crusts to vesicular appearance in an assemblage with wavellite, variscite and kaolinite

432   and occasional veins of massive turquoise in Montebras (Table 7).

433

434   Triplite [Mn_2PO_4F] – Triplite is an uncommon microscopic phase observed in Montebras

435   (Table 3).

436

437   Eosphorite [$MnAlPO_4(OH)_2•H_2O$] - Eosphorite occurs as yellowish inclusions in Montebras'

438   amblygonite and as a filling in some quartz veins where it forms subhedral crystals up to 1mm in

439   length (Table 3).

440

441   Gormanite [$Fe_3Al_4(PO_4)_4(OH)_6•2H_2O$] - In McDonalds pegmatite, numerous subhedral grains of

442   ~100 μm in amblygonite show an intense pleochroism changing from blue to greenish yellow and

443   display possibly two cleavage planes (Fig. 11). Microprobe analyses give a composition that could

444   be related to gormanite ($Fe_{2.61}Mn_{0.22}Mg_{0.13}Ca_{0.04}$)$Al_{3.92}(PO_4)_{4.12}(OH_{5.76}F_{0.24})•2.22 H_2O$ (Table 8);

445   however, the optical properties do not match exactly the gormanite-souzalite series

446   ((Fe^{2+},Mg)$_3$(Al,Fe^{3+})$_4(PO_4)_4(OH)_6•2H_2O$), Sturman et al., 1981) and the composition is not ideal, as

447   it has been observed for other tentative gormanite (Neiva et al., 2000). An alternative composition

448   would be an unknown mineral phase with the ideal composition $Fe_2Al_3(PO_4)_3(OH)_4•2H_2O$. The

449   presence of manganese with ~10% replacement of Fe could be responsible for the particularly

450   yellow pleochroic colours.

451   The occurrence of this mineral as subhedral suggests that it is formed relatively early in the

452   crystallisation sequence. However, gormanite is not stable at temperature above 390ºC (Sturman et

453   al., 1981) and both mineral possibilities are hydrated. It is therefore more likely that this phase is the

454   result of a replacement of an early Fe-rich phase (i.e. scorzalite-lazulite) as it has been observed in

455   other pegmatites (Dias et al., 2014; Roda-Robles et al., 2012).
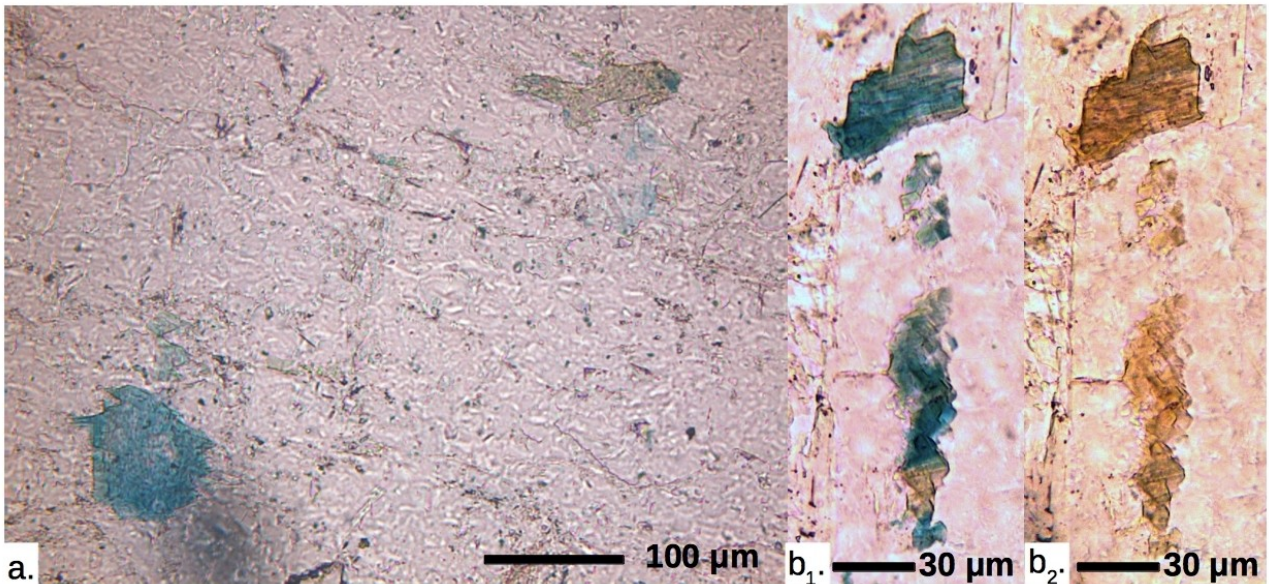
456   Figure 11. a. Grains of gormanite showing orientation with a blue pleochroism (bottom left) and beige (top right) in PPL

457   (Sample KBB3). b_1. Gormanite crystals in the maximum blue pleochroic colour displaying at least one cleavage plane and subhedral

458   shape. b_2. Same grain at 90º orientation to polarisers of b1, showing maximum yellow pleochroic colour. (Sample KBB3).

459

460

461

462

463

Table 8. Composition of gormanite

Sample phase n	KBB3 4	KBB3 3	KBB3 6
P_2O_5	35.48 (42)	37.45 (67)	36.06 (52)
Al_2O_3	24.47 (51)	25.80 (40)	24.26 (20)
FeO	24.23 (25)	22.10 (23)	23.55 (35)
MgO	0.51 (6)	0.97 (14)	0.48 (4)
MnO	2.02 (28)	1.80 (17)	2.11 (20)
CaO	0.30 (9)	0.21 (4)	0.25 (6)
Na_2O	0.14 (7)	0.28 (9)	0.12 (2)
F	0.28 (6)	0.71 (24)	0.69 (17)
H_2O	12.86 (89)	10.62 (129)	12.46 (102)
Total	100.60 (22)	100.20 (15)	100.32 (20)
Total O =F	100.49 (24)	99.90 (9)	100.03 (17)
P	4.07 (4)	4.16 (1)	4.12 (2)
Al	3.90 (7)	3.99 (2)	3.86 (3)
Fe	2.74 (3)	2.42 (1)	2.66 (3)
Mg	0.10 (1)	0.19 (3)	0.10 (1)
Mn	0.23 (3)	0.20 (2)	0.24 (2)
Ca	0.04 (1)	0.03 (1)	0.04 (1)
Na	0.04 (2)	0.07 (2)	0.03 (1)
F	0.12 (3)	0.29 (10)	0.29 (8)
OH	5.88 (3)	5.71 (10)	5.71 (8)
H_2O	2.62 (44)	1.54 (61)	2.51 (54)
Σcat.	11.13 (3)	11.06 (6)	11.05 (2)
F/(F+OH)	0.02 (0)	0.05 (2)	0.05 (1)

Gormanite calculated on 38 electrical charges
Hydroxyls calculated by difference on hydroxyl site (6-F) and charge balance
H2O calculated by difference on total measured and calculated hydroxyls groups

4.7.   Other phosphates

Churchite [*(REE)PO$_4$•2H$_2$O*] - A mineral phase identified at Bwimo-Nyarusange through conclusive X-ray diffractograms, in mixtures with crandallite group minerals.

Phase F [*Na-Al-P-F*] - Phase F occurs in lacroixite-fluorapatite veins cross-cutting viitaniemiite-bearing amblygonite in Montebras. A simplified chemical formula based on 4 anions for this phase gives Na(Al$_{0.8}$P$_{0.2}$)(F$_{3.5}$OH$_{0.5}$) which is interpreted as a phosphorus-bearing sodium aluminofluoride xerogel (See Pirard, 2022 for more details).

489 **4.8.   Non-phosphate phases**

490

491   Silicate typically found in granitic melts are found in all locations but often in negligible

492 amounts in phosphates pods. Quartz is very common as veins and cavity filling in phosphates

493 masses. It is also the main mineral in the quartzglöcke of Montebras and the quartz core of

494 Namibian localities. Quartz veins also show it is a late phase in phosphate pods of all sampling

495 sites. Feldspars (microcline and albite) are absent from most phosphate pods.

496   Muscovite is a common phase in all samples as lamellae from 0.1 to 10 mm in amblygonite and

497 often rimmed by fluorapatite. In the Habis Farm pegmatite, polylithionite is the most common mica

498 in amblygonite, also in association with fluorapatite. Samples from Habis Farm also shows small

499 amounts of pale green topaz (Table 9).

500   Kaolinite is very frequent in Montebras and Bwimo as diffuse masses between altered

501 phosphates blocks. In Bwimo, brownish veinlets of kaolinite are also present as well as small

502 rhombohedra of calcite and dolomite associated with gorceixite (Table 9).

503   In McDonalds pegmatite, 500 μm needles of corundum are present in amblygonite.

504   Cassiterite is common in Montebras and Bwimo where it was exploited as the main ore. Grains

505 are yellowish to brown, subhedral and disseminated in phosphate pods. Varlamoffite is also present

506 in quartz veins and as dark rims around stannoidite grains.

507   Small amounts of hubnerite and columbo-tantalite with ixiolite have also been observed in

508 Montebras.

Table 9. Composition of silicates

Sample	MONT2	KBB2	KBB2	MONT12	MONT15	MONT15	MONT12	BW1	BW2	BW3	BW5	MONT12	KBB2	BW2	BW2
phase	Muscovite	Lepidolite	Lepidolite	Muscovite	Muscovite	Muscovite	Muscovite	Kaolinite	Kaolinite	Kaolinite	Kaolinite	Kaolinite	Topaz	Albite	Microcline
n	3	5	5	2	2	2	3	1	2	1	2	1	3	6	2
P_2O_5	0.04 (2)	bdl	bdl	bdl	tr.	tr.	bdl	0.53	bdl	0.26	0.40 (20)	bdl	tr.	tr.	tr.
SiO_2	46.51 (91)	52.91 (78)	57.24 (279)	45.98 (85)	45.68 (74)	45.40 (60)	45.88 (35)	44.09	43.76 (5)	45.11	42.77 (113)	42.81	32.36 (33)	68.49 (22)	64.72 (36)
Al_2O_3	36.73 (27)	20.40 (83)	18.68 (300)	36.14 (20)	36.14 (16)	35.82 (104)	36.08 (23)	37.08	35.74 (111)	39.66	36.96 (79)	37.84	55.63 (29)	19.26 (21)	17.95 (18)
FeO	bdl	3.80 (42)	1.04 (53)	0.52 (1)	0.63 (14)	0.71 (57)	0.72 (2)	0.27	1.37 (27)	0.10	0.33 (6)	0.08	tr.	tr.	bdl
MnO	0.07 (6)	0.72 (14)	0.19 (4)	tr.	0.26 (10)	0.18 (3)	0.11 (1)	0.12	tr.	bdl	bdl	0.10	tr.	bdl	bdl
CuO	0.07 (3)	0.04 (6)	tr.	tr.	0.09 (13)	tr.	tr.	bdl	bdl	0.05	tr.	0.07	bdl	tr.	tr.
MgO	0.03 (2)	0.02 (1)	0.03 (2)	0.16 (4)	0.06 (0)	0.06 (3)	0.13 (1)	tr.	0.06 (4)	bdl	0.05 (3)	tr.	tr.	bdl	0.02 (1)
CaO	0.06 (4)	tr.	tr.	tr.	bdl	bdl	0.04 (3)	0.14	0.15 (11)	0.05	0.11 (5)	0.05	0.03 (2)	bdl	bdl
SrO	bdl	bdl	bdl	tr.	0.03 (4)	bdl	bdl	bdl	bdl	bdl	bdl	bdl	tr.	n.a.	n.a.
BaO	bdl	bdl	tr.	0.08 (6)	bdl	bdl	0.07 (6)	bdl	0.06 (0)	bdl	tr.	0.15	tr.	tr.	tr.
Na_2O	0.15 (2)	0.38 (5)	0.09 (4)	0.33 (7)	0.26 (13)	0.38 (13)	0.34 (3)	tr.	tr.	bdl	tr.	tr.	tr.	11.16 (13)	0.35 (5)
K_2O	10.95 (13)	10.62 (20)	10.63 (27)	10.64 (32)	10.73 (4)	10.61 (42)	11.05 (6)	tr.	0.06 (1)	0.07	0.03 (2)	bdl	tr.	0.08 (2)	16.29 (15)
F	0.86 (2)	9.23 (17)	8.91 (81)	1.43 (26)	1.31 (8)	1.31 (6)	1.39 (5)	0.07	bdl	bdl	bdl	0.17	18.92 (293)	n.a.	n.a.
H_2O	4.09 (6)		tr.	3.78 (7)	3.83 (7)	3.80 (2)	3.81 (2)	13.13	12.91 (18)	13.73	12.92 (31)	13.06	bdl	n.a.	n.a.
Total	99.62 (107)	98.16 (50)	97.10 (64)	99.43 (141)	99.09 (71)	98.72 (14)	99.72 (50)	95.51	94.18 (111)	99.06	93.76 (242)	94.37	107.57 (318)	99.21 (29)	99.58 (56)
Total O =F	99.26 (107)	94.28 (43)	93.35 (83)	98.83 (130)	98.54 (75)	98.17 (16)	99.14 (48)	95.48	94.18 (111)	99.06	93.75 (240)	94.31	99.60 (196)	99.21 (29)	99.58 (56)
P	bdl	bdl	bdl	bdl	bdl	bdl	bdl	tr.	bdl	tr.	0.02 (1)	bdl	tr.	bdl	bdl
Si	3.10 (2)	3.78 (4)	4.05 (21)	3.09 (2)	3.08 (3)	3.08 (4)	3.08 (0)	2.01	2.03 (3)	1.97	1.98 (0)	1.96	0.99 (1)	3.01 (1)	3.01 (1)
Al	2.88 (2)	1.72 (8)	1.55 (25)	2.86 (2)	2.87 (4)	2.86 (9)	2.86 (0)	1.99	1.96 (3)	2.04	2.02 (1)	2.05	2.01 (1)	1.00 (1)	0.98 (1)
Fe	bdl	0.23 (2)	0.06 (3)	0.03 (0)	0.04 (1)	0.04 (3)	0.04 (0)	0.01	0.05 (1)	bdl	0.01 (0)	bdl	bdl	bdl	bdl
Mn	bdl	0.04 (1)	0.01 (0)	tr.	bdl	0.01 (0)	0.01 (0)	bdl	bdl	bdl	bdl	bdl	bdl	bdl	bdl
Cu	bdl	bdl	bdl	bdl	bdl	bdl	bdl	bdl	bdl	bdl	bdl	bdl	bdl	bdl	bdl
Mg	bdl	bdl	bdl	0.02 (0)	0.01 (0)	0.01 (0)	0.01 (0)	bdl	bdl	bdl	0.01 (0)	bdl	bdl	bdl	bdl
Ca	bdl	bdl	bdl	bdl	bdl	bdl	bdl	0.01	tr.	bdl	bdl	bdl	bdl	bdl	bdl
Sr	bdl	bdl	bdl	bdl	bdl	bdl	bdl	bdl	bdl	bdl	bdl	bdl	bdl	n.a.	n.a.
Ba	bdl	bdl	bdl	bdl	bdl	bdl	bdl	bdl	bdl	bdl	bdl	bdl	bdl	bdl	bdl
Na	0.02 (0)	0.05 (1)	tr.	0.04 (1)	0.03 (2)	0.05 (2)	0.04 (0)	bdl	bdl	bdl	bdl	bdl	bdl	0.95 (1)	0.03 (0)
K	0.93 (2)	0.97 (2)	0.96 (2)	0.91 (4)	0.92 (0)	0.92 (3)	0.95 (1)	bdl	bdl	bdl	bdl	bdl	bdl	bdl	0.97 (0)
F	0.18 (1)	2.09 (3)	1.99 (19)	0.30 (5)	0.28 (2)	0.28 (1)	0.29 (1)	tr.	bdl	bdl	bdl	0.02	2.00 (2)	n.a.	n.a.
OH	1.82 (1)	bdl	tr.	1.70 (5)	1.72 (2)	1.72 (1)	1.71 (1)	3.99	4.00 (0)	4.00	4.00 (0)	4.00	n.a.	n.a.	n.a.
H_2O															
Σcat.	6.95 (2)	6.80 (2)	6.65 (7)	6.98 (0)	6.98 (2)	6.99 (3)	7.00 (1)	4.05	4.06 (0)	4.03	4.05 (1)	4.03	3.02 (2)	4.97 (1)	5.00 (0)
F/(F+OH)	0.09 (0)	1.00 (0)	0.96 (5)	0.15 (3)	0.14 (1)	0.14 (1)	0.15 (0)	0.00	0.00 (0)	0.00	0.00 (0)	0.01			

Micas calculated on 22 electrical charges - Hydroxyls calculated by difference on hydroxyl site (2-F)

510   **5.   Alteration of aluminium phosphates**

511

512   The complexity of aluminium phosphates pods mineral assemblages in pegmatites is mostly the

513   result of the post-magmatic alteration process, although some minor mineral phases (topaz, Fe-Mn

514   phosphates) could be of magmatic crystallisation and associated with the formation of primary

515   amblygonite, it appears that in the studied pegmatites Na-bearing and most (Ca, Sr, Ba) minerals are

516   the result of metasomatic and hydrothermal replacements and precipitation while metal-free

517   hydrated aluminium-phosphates are linked to relatively low-temperature alteration processes (Fig.

518   12, 13).
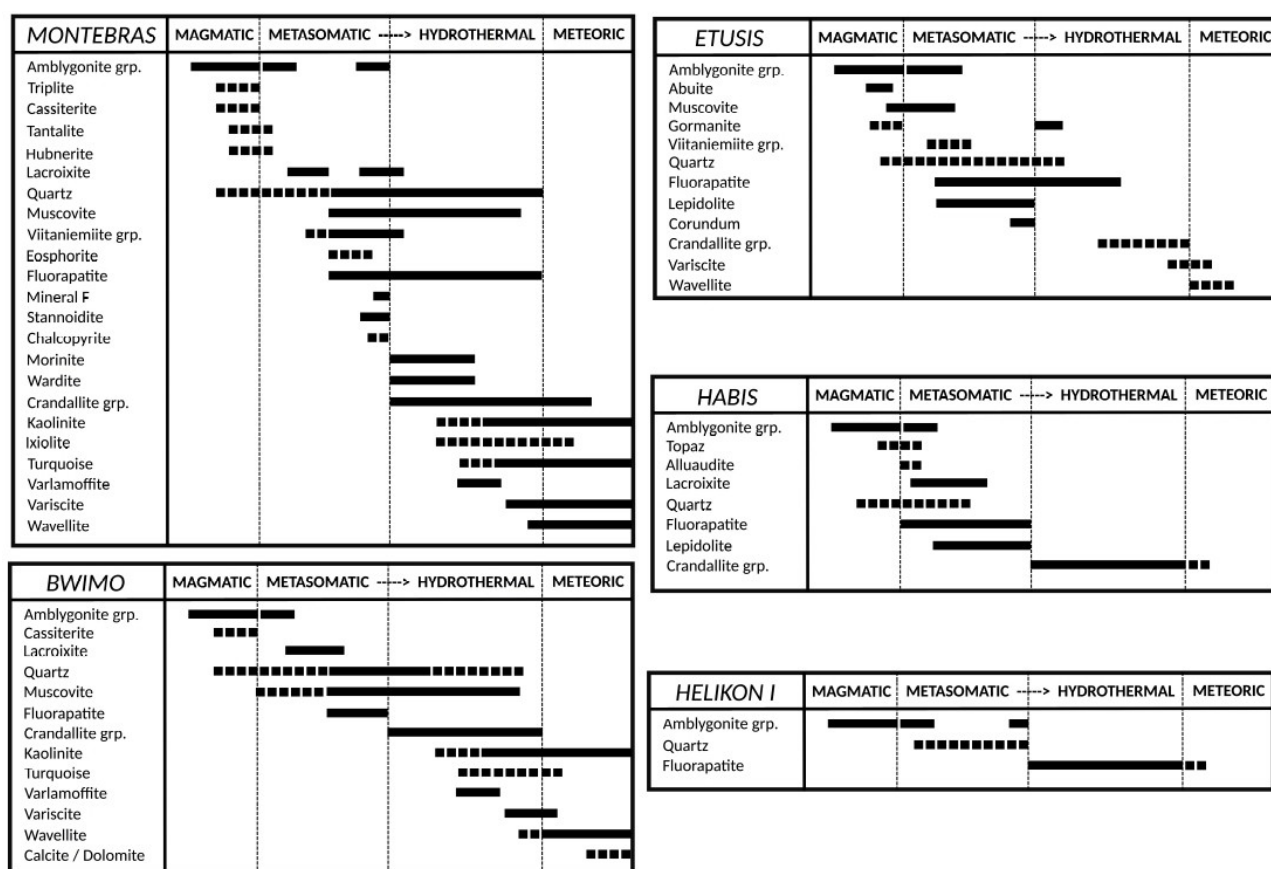
519   Figure 12. Paragenetic sequences of phosphates mineral assemblages in Montebras, Bwimo and Namibian localities. The

520   transition metasomatic/hydrothermal is unclear and broadly defined as a change from deep replacement reactions to direct

521   precipitation in open spaces and surface replacement. Dotted lines are mineral phases with limited paragenetic constrains.

522

523

5.1. Magmatic conditions

524

525

526   The Montebras pegmatite is an excellent case of study to establish the conditions required for

527   the formation of amblygonite-montebrasite phosphates pods. Many pegmatites do not have

528   preserved analogous parental melts or potentially quenched materials and therefore some

529   hypotheses have to be made on the crystallization process. Montebras pegmatitic cupola and

530   surrounding magmatic outcrops happens to provide such information. For the magmatic stage, we

531   assume here that amblygonite-montebrasite masses in other nearby sampled localities have a small-

532   scale crystallization process broadly similar to Montebras.

533   The Montebras pegmatite is a cupola formed by the residual melts of the Montebras

534   microgranite, accumulated against the roof formed by the surrounding Chanon granite (Aubert,

535   1969). Early modelling of the microgranite composition gave a highly alkaline ($(Na_2O + K_2O +$

536     $Li_2O) = 9$ wt.%) liquid with up to 0.5 wt.% Li_2O and up to 1 wt.% F (Aubert, 1969). Such

537   composition is similar to the nearby Richemont rhyolite (Raimbault & Burnol, 1998) which

538   contains 1.3 wt.% F, 0.7 wt.% Li_2O and 1.2 wt.% P_2O_5, and is a likely quenched analogue to the

539   Montebras leucogranite. The bulk composition of this magma agrees with geochemical

540   requirements for the development of this type of Li-Cs-Ta pegmatite melt (Charoy and Noronha,

541   1999) starting with a peraluminous felsic parental melt, rich in sodium and poor in Ca, Fe and Mg

542   while P and F are high to very high.

543   The high fluorine content in the original melt allows the eutectic point of this magmatic system

544   to shift towards albite (Manning, 1981), increasing the sodium concentration in the evolved melt

545   along with F, P, B, Sn, Nb, Ta and forming the albite leucogranite of Montebras (Pal et al., 2007;

546   Neiva and Ramos, 2010). The crystallisation of quartz and alkali feldspars in the magma chamber

547   lead to a volatile enrichment in the residual melt forming a low viscosity and high diffusivity liquid

548   and allowing potential extreme fractionation (London, 1992). In such liquids, the precipitation of

549   topaz and the incorporation of phosphorus in feldspar is hindered by the stability of Al-P-F

550   complexes in the residual melt and as a consequence, high phosphate contents in melts enhance the

551   stability of quartz over feldspar (Webster et al., 1997), leading to important silica precipitation and a

552   trend towards a probable melt-melt immiscibility (Raimbault and Burnol, 1998; Thomas et al.,

553   2006). Such immiscibility could have occurred in the cupola between Si-rich and F-rich melts. In

554   this process, phosphorus will preferentially partition into the fluorinated phase, providing a very

555   low solidus for the phosphate-rich melts (Gramenitsky and Shehekina, 1993; Webster et al., 1997).

556   The crystallisation temperature of the Montebras microgranite is likely to be like other local

557   intrusions such as Richemont rhyolite and Beauvoir granite that have a consolidation temperature of

558   ~550°C (Raimbault & Burnol, 1998; Pichavant et al., 1987). The texture and abundance of

559   amblygonite-montebrasite indicates that it is a primary magmatic phase in Montebras and this

560   interpretation is confirmed by the presence of phenocrysts of amblygonite and triplite in Richemont

561   rhyolite glass (Raimbault & Burnol, 1998) and in melt inclusions in pegmatitic quartz (Thomas et

562   al., 2006) despite the poor nucleation characteristics associated with amblygonite-montebrasite

563   (London et al., 2001). Montebras amblygonite pods and accessory triplite are included in a quartz-

564   rich environment and are possibly the macroscopic result of this melt-melt immiscibility. In

565   Namibia, pegmatite bodies are emplaced as dykes produced from a main intrusion precipitating

566   quartz and feldspar and phosphate primary crystallisation occurs in the quartz core of such dykes.

567   The separation between a phosphorus-rich melt and a mostly silicate-rich melt in a highly-

568   fluorinated environment is also responsible in hindering the formation of lithium aluminosilicates

569   (London and Burt, 1982; London et al., 1999) in favour of lithium aluminophosphates. The primary

570   amblygonite preserved in phosphate pods provides an estimation of the fluorine content in the

571   phosphorus-rich melt based on partition coefficient (London et al., 2001). Montebras primary

572   amblygonite ($Amb_{0.8}Mnt_{0.2}$) is in equilibrium with an haplogranitic melt containing at least ~3 wt.%

573   F. In a context of melt-melt immiscibility, this fluorine concentration would represent the bulk

574   composition of an equilibrated pegmatitic system where ~66% of quartz and feldspars would habe

575   be fractionated from the parental melt. In Namibian pegmatites, slightly lower (and more robustly

576   determined (London et al., 2001)) fluorine content in melts (between 2 and 3 wt.% F) could suggest

577   that melt-melt immiscibility did not occur. Bwimo is considerably less F-rich with a pegmatitic melt

578   likely to be below 1 wt.% F. In Montebras, calcium concentration is relatively low in the parental

579   melt and fractionation process would not enrich this element in the residual melt, therefore

580   fluorapatite does not appear as an abundant primary phase. In Etusis McDonald's pegmatite of

581   Namibia, the texture and composition of abuite suggest that it could be a primary high-temperature

582   Ca-bearing phase as it has been suggested for its hydrated analogue gatumbaite (Duggan et al.,

583   1990). This would be a different process of formation for this mineral as the only other locality

584   where abuite is found is the result of hydrothermal alteration of a augelite+berlinite+trolleite

585   pyroclastic rock (Matsubara et al., 1999).

586

587   **5.2.   Metasomatic stage**

588

589   As this volatile-rich magma nears its solidus, a retrograde ebullition process is likely to start and

590   leads to further unmixing (London and Burt, 1982; Webster et al., 1997; Charoy & Noronha, 1999;

591   Baldwin et al., 2000). Based on the fluorine concentration of the Richemont rhyolite, the water

592   content would be at least 4-6 wt.% when amblygonite crystallises. In the supercooled conditions of

593   this fluid-rich melt at intrusion depth (<1 kbar), this is above the water saturation of such

594   haplogranitic melt and exsolution of aqueous fluids occurs. The melt-fluid exsolution process is

595   non-congruent for fluorine and dependent on several parameters (Webster, 1990) indicating that a

596   considerable amount of fluorine would partition in the aqueous phase where it would reach very

597   high values as well as a high lithium content (1-2 wt.%) and sodium (~10 wt.%) (Harlaux et al.,

598   2017) helped by the supercritical nature of the fluid. Secondary amblygonite could form by

599   reequilibration of the primary phase with a water-rich fluid rather than a melt, sufficiently rich in

600   lithium to only be limited to a F-OH exchange. Such replacement seems to be common in

601   pegmatites (Cerna et al., 1972; Kallio, 1978, Baldwin et al., 2000; Lefevre, 2003) and could be a

602   potential marker of the magmatic-hydrothermal transition when aqueous fluids are exsolved out of

603   the residual magma. As the F-rich aqueous fluid rapidly change its composition, it is altering

604   silicates and remobilising large amount of sodium leading to the albitisation of the cupola. The most

605   obvious reaction formed by these high temperature aqueous fluids in phosphate pods is the

606   replacement of primary and secondary amblygonite by lacroixite as a result of a simple $Li^+ \rightarrow Na^+$

607   replacement. Textural evidence shows that the hypothetical high temperature phase $(Li,Na)AlPO_4F$

608   breakdown upon cooling is not occurring and that meshy lacroixite textures are clearly a secondary

609   process, confirming the absence of Li-Na substitution in the amblygonite-montebrasite series (Groat

610   et al., 1990). No magmatic lacroixite, as observed in experimental studies and melt inclusions

611   (London et al., 1989, 1998, 1999) has been observed in this study.

612   As temperature decreases (~400ºC (Merceron et al., 1987)), melt is no longer present and fluids

613   are mobilised through a network of open veins where quartz, muscovite, eosphorite, apatite and

614   significant amounts of lacroixite precipitate from a Na-Al-P-F-rich fluid. The small amount of

615   lithium still present in the aqueous fluid allow the formation of F-poor montebrasite in veins. The

616   precipitation of ternary montebrasite from an aqueous fluid is supported by trace elements patterns

617   showing a considerable enrichment in medium rare earth elements as a probable consequence of an

618   enhanced REE tetrad effect in montebrasite precipitated from a Al-F-rich aqueous fluid (Veksler et

619   al., 2005) compared to the equivalent hydrous melt. The high concentration of fluorine still present

620   in the fluids allow the crystallisation of more lacroixite, viitaniemiite-like minerals and phase F in

621   some veins. High fluorine, along with seemingly high phosphorus activity also prevent the late

622   formation of lithium aluminosilicates and rather form the observed assemblage of tertiary

623   amblygonite-montebrasite and quartz that act to prevent the formation of lepidolites (Charoy and

624   Noronha, 1999) and topaz, despite being common phases in the albite granite at Montebras.

625   Although phase F has an undetermined nature, it is not excluded that its formation could be the

626   result of the survival of a very low temperature (~400ºC) fluoride melt (Vasyukova & Willams-

627   Jones, 2014, 2016; Veksler et al., 2012; Klemme 2004, Wyllie & Tuttle, 1961). However, auto-

628   metasomatism during albite granite greisenisation and albitisation could also lead to the production

629   of Na- and F-rich fluids accumulated in the cupola and precipitating in cooler conditions, in a

630   process similar to the formation of cryolite and chiolite (Butuzov et al., 1971; Bailey, 1980). This

631   latter metasomatic reaction could also be the origin of viitaniemiite-like mineral from a fluid rich in

632   Na, Ca and F altering eosphorite. Such association of viitaniemiite + eosphorite + montebrasite is

633   known from Eräjärvi (Lahti, 1981).

634   Calcium activity increases in aqueous fluids as the system further cools and calcium becomes

635   involved in many metasomatic reactions. Fluorapatite, which is not abundant or simply absent in the

636   primary phosphate assemblage, becomes very frequent in all studied pegmatites at this stage,

637   precipitating as a Mn-rich variety in open cavities filled with quartz and micas and in veinlets cross-

638   cutting amblygonite + lacroixite masses. Apatite replacing directly earlier phosphates is typically

639   Mn-poor and is possibly happening earlier than Mn-rich apatites. At these temperature conditions,

640   augelite and trolleite could be common potential phases; however, the abundance of sodium and

641   calcium solutes in aqueous fluids prevent the formation of cation-free aluminophosphates (London

642   and Burt, 1982). In Etusis pegmatite (Namibia), fluorapatite replacement of amblygonite is also

643   accompanied by corundum and some muscovite, suggesting that temperatures remains above 350-

644   400ºC (Kennedy, 1959).

Temperature (°C)	850	800	750	700	650	600	550	500	450	400	350	300	250	200	150	100	50
Petrogenetic Process	Cotectic Qz+Or	'Eutectic' Qz+Or+Ab			Immiscibility Si >< Al-P-F		Retrograde Ebullition			Increasing Ca activity			Decreasing (and fluctuating) pH			Kaolinisation Oxidation	
						Albitization		Greisenization			Sericitisation						
Phosphate Pods					Primary Amblygonite		Secondary Amblygonite		Tertiary Montebrasite	Apatite	Quartz	Crandallites Ca-Sr				Wavellite Variscite	
						Diffuse Lacroixite	Veined Lacroixite		Viitaniemiite	Morinite			Crandallites Ba-REE			Turquoise	
									Fluorides *s.l.*	Wardite	Micas *s.l.*					Kaolinite	
Silicate Pegmatite	Quartz Orthoclase	Quartz Orthoclase Albite			Massive Quartz		Albite (Sulfides)		Muscovite Lepidolite		Sericite					Kaolinite	
					W-Nb-Ta-Sn minerals												
Melts & Fluids	Haplogranitic hydrous peraluminous ~1 wt.% F ~1 wt.% P₂O₅ ~0.5 wt.% Li₂O <1 wt.% CaO	Na-rich haplogranitic			F-rich melt >3 wt.% F 4-6 wt.% H₂O + Si-rich melt		F-rich supercritical fluid ~10 wt.% Na₂O 1-2 wt.% Li₂O + residual melt			Ca-Sr-Ba rich Si-rich supercritical fluid			Aqueous fluid			Meteoric Aqueous fluid	

Figure 13. Tentative evolution of aluminium phosphate pods mineralogy and their direct silicate environment during magmatic crystallisation and subsequent cooling and their relationship with possible petrological processes. Variation from this sequence can occurs right from the beginning depending on the evolution of the primary melt and the role played by some parameters such as the content in fluorine and water and for specific mineral phases, initial concentrations such as calcium or sodium.

5.3. Hydrothermal phase

The distinction between metasomatic and hydrothermal phase in this study is set when high temperature replacement reactions of primary phases become negligible compared to direct precipitation in open veins. The combined presence of sodium and calcium in hydrothermal fluids below 400ºC lead to the formation of morinite and wardite in open vugs. However, these two hydrated minerals seem to become unstable with further hydrothermalism and are often replaced by apatite and crandallite group minerals, notably resulting in pseudomorphs of wardite and morinite crystals into Na-rich fibrous and fine-grained fluorapatite. These reactions have been observed experimentally and described as "nafalapatite" (Fisher & McConnell, 1969) where morinite thermal destabilisation product is an assemblage of Na-bearing fluorapatite and Na-Al fluorides (Fisher & Volborth, 1960). This latter reaction product could be an alternative process for the precipitation of phase F, although low temperatures tend to produce hydrated fluorides (Bailey, 1980). The seemingly frequent alteration of morinite and wardite into Na-rich apatite at Montebras could partly

664   explain the rarity of these minerals in many deposits where fluorapatite, crandallite and hydrated

665   aluminium phosphates abound.

666   Hydrothermal alteration of feldspars to sericite and kaolinite frees significant amounts of Ca, Sr

667   and Ba that are remobilised to form crandallite group minerals at temperature below 300ºC

668   (Schreyer, 1987; Dill, 2001). It has been suggested that leaching from the country rock is the main

669   source for these elements (Galliski et al., 2012; Charoy and Noronha, 1999), however, the

670   widespread presence of these minerals (particularly goyazite and gorceixite) in intrusions occurring

671   in a variety of host rocks suggests otherwise. Percolating fluids precipitate massive amounts of Ca-

672   Sr crandallite in veins through the primary phosphate pods, but also in morinite and apatite-filled

673   vugs where Ca-Sr crandallite occurs as zoned rhombohedra of Sr-rich crandallite ($Cn_{0.8}Gz_{0.2}$) and

674   goyazite ($Gz_{0.9}Cn_{0.1}$). The variation in Ca and Sr concentration in crandallite s.l. and the formation

675   of apatite is likely to be related to pH variations in fluids as these minerals are particularly sensitive

676   to these conditions (Dill et al., 1991; Schwab et al., 1996). Changes to lower pH and lower

677   temperatures favours 12-fold coordination for alkaline-earth elements and prevent the formation of

678   fluorapatite (Blanchard, 1972). Sericitization of feldspars could also be the source for the late

679   precipitation of silica in veins crossing through phosphates pods.

680   In Montebras and Bwimo, gorceixite is particularly associated with kaolinite veins where

681   kaolinite acts as a catalyst for the precipitation of Ba- and REE-rich crandallites (Schwab et al.,

682   1990; Gilkes and Palmer, 1983). The conditions required for the formation of kaolinite and

683   gorceixite are likely to be relatively low temperature (~100ºC) fluids with oxidising and acidic

684   conditions (Nicolas and de Rosen, 1963). Acidic fluids (pH < 6) explain the absence of fluorapatite

685   precipitation despite fluorine being leached out of amblygonite (Latil and Maury, 1977) and calcium

686   readily available. In the absence of a major F-hosting phase, gorceixite and florencite contains

687   considerable amount of fluorine. The hypothesis that Ba-F mineralisation precipitated as barite and

688   fluorite is a regional event occuring millions of years after magmatic events in Montebras (Marcoux

689   et al., 2021) is not fully supported in our data as gorceixite seems to occur in the same petrogenetic

690   step at Montebras and Bwimo.

691   The percolation of acidic hydrothermal fluids in the pegmatite also affect the tin ore and

692   particularly copper hosted in stannoidite and chalcopyrite that is leached out to form turquoise in

693   quartz veins. The destabilisation of stannoidite forms a Sn-rich gel that precipitates as varlamoffite,

694   as described for stannite at temperature below 350ºC (Bonnici et al., 1964).

695

696   **5.4.   Meteoric phase**

697

698   At low temperature (<100ºC), variscite, wavellite and kaolinite become the dominant

699   paragenesis in Montebras and Bwimo localities. Veins of variscite and its association with turquoise

700   suggests that it appears in the latest part of the hydrothermal phase when temperatures drop below

701   130ºC (Drüppel et al., 2007) and fluids no longer carry large amounts of solutes. The shift from

702   variscite to wavellite precipitation is related to another decrease in pH (Blount, 1974; Dill, 2001)

703   and possibly temperature (Drüppel et al., 2007) that would also prevent the formation of late apatite

704   in favour of crandallite (Stoffregen and Alpers, 1987; Dill et al., 1991, PePiper and Dolansky,

705   2005). Succession of crandallite and clay-wavellite layers observed in the alteration crust of

706   phosphate pods could relate to variations in the sub-surface hydrous regime and seasonal changes

707   (Capdecomme, 1952; Van Riemsdijk et al, 1975; Schwab et al. 1990; Dill, 2001). In Bwimo, the

708   equatorial climate considerably leached the soil, which has the effect of producing a lateritic

709   ferricrete typically formed of goethite, gibbsite and kaolinite on silicate rocks. In Fe-poor

710   phosphate-rich nodules, wavellite and kaolinite become the main residual products and crandallite

711   group minerals, although supposed to be abundant in equatorial climate (Dill, 2001) seems to be

712   equally leached out. In temperate climate such as Montebras, wavellite alteration is not as pervasive

713   and tend to form crust and fillings. In the desert climate of Namibia, wavellite is present but its

714   distribution is very unequal and subject to the local surface features of the deposit and mining

715   activity. The most common meteoric alteration observed on Namibian samples is a thin crust of

716   hydroxylapatite partly consumed by crandallite, directly growing on altered amblygonite.

717

718

719   **6. <u>Conclusions</u>**

720

721   When Fe-Mn-Mg are absent from the phosphatic pods of a pegmatite body, the magmatic and

722   hydrothermal evolution of aluminium phosphate is very similar between intrusions. The initial

723   crystallisation of amblygonite or F-rich montebrasite at the magmatic stage and temperature of

724   ~550ºC is followed by a progressive F→OH replacement inside the primary amblygonite by fluids,

725   followed by a Li-leaching event associated with Na-metasomatism characterised by the pervasive

726   alteration into lacroixite. The fracturing of the rock after complete consolidation leads to Na-Al-P-F

727   rich fluids to percolate in the pegmatite and deposit additional lacroixite and some fluorapatite. As

728   greisenisation and albitisation occurs in the main granitic body, Na, Ca, Sr and Ba are freed from

729   feldspars and micas and deposit Na-Ca phosphates (wardite, morinite) and Ca-phosphates

730   (fluorapatite) at temperatures of 350-400ºC.

731   The percolating aqueous fluids cool down and become progressively acidic, helping crandallite

732   group minerals (crandallite, goyazite, gorceixite, florencite) to form and leaching copper out of

733   sulfides, which can eventually be deposited as turquoise. In the presence of high concentration of

734   alkali-metals in fluids, minerals such as augelite, trolleiite and berlinite do not seem to form at any

735   stage during the alteration and its only at lower temperature that phases such as variscite and

736   wavellite can occur.

737   The last step in alteration sequences of aluminium phosphates is the direct weathering of

738   exposed outcrops, where climate has a considerable effect. In dry conditions (Namibia) do not allow

739 extensive weathering of phosphates (minimal hydroxylapatite and crandallite), while temperate

740 (France) and tropical humid (Rwanda) conditions allow the formation of considerable amounts of

741 kaolinite. In tropical conditions however, the relatively barren and highly acidic meteoric waters

742 limits the late paragenesis to kaolinite and minor amounts of wavellite while temperate climate

743 displays a more complex assemblage (variscite, wavellite, turquoise, crandallite group).

744

745

746 **7. <u>Acknowledgments</u>**

750

751

752 **8. <u>References</u>**

753

754 Aubert, G., 1969. Les coupoles granitiques de Montebras et d'Echassières (Massif Central français)

755 et la genèse de leur minéralisation étain-lithium-tungstène-béryllium. *Mémoire du BRGM*, **46**, 354p.

756 Bailey, J.C., 1980. Formation of cryolite and other aluminofluorides: a petrologic review. *Bulletin*

757 *of the Geological Society of Denmark*, **29**, p1-45.

758 Baldwin, J.R., Hill, P.G., von Knorring, O. & Oliver, G.J.H., 2000. Exotic aluminium phosphates,

759 natromontebrasite, brazilianite, goyazite, gorceixite and crandallite from rare-element pegmatites in

760 Namibia. *Mineralogical Magazine*, **64(6)**, p1147-1164.

761 Blanchard, F.N., 1972. Physical and chemical data for crandallite from Alachua County, Florida.

762 *American Mineralogist*, **57**, p473-484

763 Blount, A.M., 1974. The crystal structure of crandallite. *American Mineralogist*, **59**, p41-47

764 Bonnici, J.-P., Doucet, S., Goni, J. & Picot, P., 1964. Etude geochimique et mineralogisque sur la

765 degradation de la cassiterite. Evolution du gel qui en derive (Varlamoffite). *Bulletin de la Societe*

766 *francaise de Mineralogie et de Cristallographie*, **87**, p355-364.

767 BRGM (Guillou, Y. & Ziserman, A.), 1987. Plan Mineral du Rwanda. *Ministere de l'industrie, des*

768 *mines et de l'Artisanat, Republique Rwandaise*, Orleans, 580p, 75 figures, 17maps.

769 Burnham, C.W., 1991. LCLSQ version 8.4., least-squares refinement of crystallographic lattice

770 parameters. *Department of Earth and Planetary Sciences*. Harvard University.

771 Butuzov, B.P., Khetchikov, L.N. & Shaposhnikov, A.A., 1971. Inclusions in synthetic crystals and

772 their significance in thermobarometry of minerals. *In*: N.P. Ermakov & L.N. Khetchikov (eds),

773 *Investigations of mineral-forming solutions and melts in inclusions in minerals* (Tr.) Vses Nauchno-

774 Issled. Inst. Sint. Miner. Syrya, **14**, p7-14.

775 Cahen, L. & Ledent, D., 1979. Precisions sur l'age, la petrogenese et la position stratigraphique des

776 'granites a etain' de l'Est de l'Afrique centrale. *Bulletin de la Societe belge de Geologie*, **88**, 1, p33-

777 49.

778 Capdecomme, L., 1952. Sur les phosphates alumineux de la region de Thies (Senegal). *Comptes*

779 *Rendus de l'Academie des Sciences*, **234**, p1377(p187-189).

780 Cerna, I., Cerny, P. & Ferguson, R.B., 1972. The Tanco pegmatite at Bernic Lake, Manitoba. III.

781 Amblygonite-Montebrasite. *The Canadian Mineralogist*, **11**, p643-659.

782 Charoy, B. & Noronha, F., 1999. Rare-element (Li-rich) granitic and pegmatitic plutons: a primary

783 or superimposed signature. *Revista Brasileira de Geociencias*, **29(1)**, p3-8.

784 Dias, P.A., Leal Gomes, C., Guimaraes, F. & Hatert, F., 2014. Wyllieite reaction coronas on

785 scorzalite in pegmatite dykes. *IMA 2014*, 1-5 September 2014, Gaetang, South Africa.

786 Diehl, B. J. M., 1992. Lithium Caesium Beryllium. Open File Report, Mineral Ressource Series.

787 *Geological Survey of Namibia*, Windhoek, 18p.

788 Dill, H.G., 2001. The geology of aluminium phosphates and sulphates of the alunite group minerals:

789 a review. *Earth-Science Reviews*, **53**, p35-93.

790 Dill, H.G., Busch, K. & Blum, N., 1991. Chemistry and origin of vein-like phosphate

791 mineralization, Nuba Mts (Sudan). *Ore Geology Review*, **6**, p9-24.

792 Drüppel, K., Hosch, A. & Franz, G., 2007. The system Al_2O_3-P_2O_5-H_2O at temperatures below

793 200ºC: Experimental data on the stability of variscite and metavariscite $AlPO_4.2H_2O$. *American*

794 *Mineralogist*, **92**, p1695-1703.

795 Duggan. M.B., Jones, M.T., Richards, D.N.G. & Kamprad, J.L., 1990. Phosphate minerals in altered

796 andesite from Mount Perry, Queensland, Australia. *The Canadian Mineralogist*, **28**, p125-131.

797 Enju, S., & Uehara, S.. 2015. Abuite, IMA2014-084. CNMNC Newsletter No. 23, Feb 2015.

798 *Mineralogical Magazine*, **79**, p51-58.

799 Fisher, D.J. & Volborth, A., 1960. Morinite-Apatite-Whitlockite. *American Mineralogist*, **45**, p645-

800 667.

801 Fisher, D.J. & McConnell, D., 1969. Aluminium-rich Apatite. *Science*, **164**, p551-553.

802 Fransolet, A.-M., 2007. Phosphate associations in the granitic pegmatites: the relevant significance

803 of these accessory minerals. *Granitic Pegmatites: The State of the Art* – International Symposium,

804 6-12th of May 2007, Porto, Portugal.

805 Galliski, M. A., Cerny, P., Marquez-Zavalia, M. F. & Chapman, R., 2012. An association of

806 secondary Al-Li-Be-Ca-Sr phosphates in the San Elias Pegmatite, San Luis, Argentina. *The*

807 *Canadian Mineralogist*, **50**, p933-942.

808 Gilkes, R.J. & Palmer, B., 1983. Synthesis, properties and dehydroxylation of members of the

809 crandallite-goyazite series. *Mineralogical Magazine*, **47**, p221-227.

810 Gramenitsky, Y. N., Shekina, T. I., Berman, I.B. & Popenko, D.P., 1993. Concentration of lithium

811 by aluminofluoride melt in granitic system containing fluorine. *Transaction of the Russian Academy*

812 *of Sciences*, **331,** p.139-144.

813 Groat, L. A., Raudsepp, M., Hawthorne, F. C., Ercit, T. S., Sherriff, B. L. & Hartman, J. S., 1990.

814 The amblygonite-montebrasite series: Characterization by single-crystal structure refinement,

815 infrared spectroscopy, and multinuclear MAS-NMR spectroscopy. *American Mineralogist*, **75**,

816 p992-1008..

817 Harlaux, M., Mercadier, J., Bonzi, W. M.-E., Krmer, V., Marignac, C. & Cuney, M., 2017.

818 Geochemical signature of magmatic-hydrothermal fluids exsolved from the Beauvoir rare-metal

819 granite (Massif Central, France): Insights from LA-ICPMS analysis of primary fluid inclusions.

820 *Geofluids*, **2017**, 25p.

821 Hatert, F., Fransolet, A.-M. & Maresch, W.V., 2006. The stability of primary alluaudites in grnaitic

822 pegmatites: an experimental investigation of the $Na_2(Mn_{2-2x}Fe_{1+2x})(PO_4)_3$ system. *Contributions to*

823 *Mineralogy and Petrology*, **152**, p399-419.

824 Kallio, P., 1978. A new X-ray method for the estimation of fluorine content in montebrasites.

825 *American Mineralogist*, **63**, p1249-1251.

826 Keller, P., 1991. The occurrence of Li-Fe-Mn phosphate minerals in granitic pegmatites of Nambia.

827 *Communications of the Geological Survey of Namibia*, **7**, p21-34.

828 Kennedy, G. C., 1959. Phase relations in the system Al_2O_3 at high temperatures and pressures.

829 *American Journal of Science*, **257**, p563-573.

830   Klemme, S. 2004. Evidence for fluoride melts in Earth's mantle formed by liquid immiscibility.

831 *Geology*, **32(5)**, p441-444.

832 Lacroix, A., 1891. Note préliminaire sur un minéral nouveau de Montebras (Creuse). *Bulletin de la*

833 *Société française de Minéralogie*, **14**, p187-189.

834 Lacroix, A., 1910. Minéralogie de France et de ses colonies, T.4., *Béranger*, Paris, 923p.

835 Lahti, S.I., 1981. On the granitic pegmatites of Eräjärvi area in Orivesi, Southern Finland.

836 *Geological Survey of Finland*, **314**, 82p.

837   Latil.C. & Maury, R., 1977. Contributions a l'etude des echanges d'ions OH-, Cl-, F- et de leur

838   fixation dans les apatites hydrothermales. *Bulletin de la Societe Francaise de Mineralogie et de*

839   *Cristallographie.* **100**, p246-250.

840   Lefevre, P., 2003. Contribution a l'etude mineralogique et petrographique des associations des

841   phosphates d'aluminium des pegmatites de Rubindi et Kabilizi (Rwanda). *M.Sc. Thesis*, University

842   of Liege, 68p.

843   London, D., 1992. Phosphorus in S-type magmas: the P_2O_5 content of feldspars from peraluminous

844   granites, pegmatites and rhyolites. *American Mineralogist*, **77**, p126-145.

845   London, D. & Burt, D.M., 1982. Chemical models for lithium aluminosilicates stabilities in

846   pegmatites and granites. *American Mineralogist*, **67**, p494-509.

847   London, D., Morgan VI, G.B. & Hervig, R.L., 1989. Vapor-undersaturated experiments with

848   Macusani glass + H_2O at 200MPa, and the internal differentiation of granitic pegmatites.

849   *Contributions to Mineralogy and Petrology*, **102**, p1-17.

850   London, D., Morgan VI, G.B. & Icenhower, J., 1998. Stability and solubility of pollucite in the

851   granite system at 200MPa H_2O. *The Canadian Mineralogist*, **36(2)**, p497-510.

852   London, D., Wolf, M.B., Morgan VI, G.B. & Gallego Garrido, M., 1999. Experimental silicate-

853   phosphate equilibria in peraluminous granitic magmas with a case study of the Albuquerque

854   batholith at Tres Arroyos, Badajoz, Spain. *Journal of Petrology*, **40**, p215-240.

855   London, D., Morgan VI, G.B. & Wolf, M.B., 2001. Amblygonite-Montebrasite solid solution as

856   monitors of fluorine in evolved granitic and pegmatitic melts. *American Mineralogist*, **86**, p225-

857   233.

858   Manning, D. A. C., 1981. The effect of fluorine on liquidus phase relationships in the system Qz-

859   Ab-Or with excess water at 1kb. *Contributions to Mineralogy and Petrology*, **76**, p206-215.

860   Marcoux, E., Barré, B., Pichavant, M. & Poujol, M., 2021. Age et genese de la coupole granitique a

861   métaux rares (sn, Li, Nb-Ta, W) de Montebras (Creuse, Massif central français). *Earth Sciences*

862   *Bulletin*, **192(16)**, 33p.

863   Mason, B., 1941. Minerals of the Varutrask pegmatite. XXIII. Some iron-manganese phosphate

864   minerals and their alteration products, woth special reference to material from Varutriisk. **63**, p117-

865   165.

866   Matsubara, S., Kato, A., Takada, M. & Miyawaki, R. 1999. Trolleite-augelite pseudomorphs

867   supposed after berlinite from the Hinomaru-Nako mine, Yamaguchi Prefecture, western Japan.

868   *Mineralogical Journal*, **21(4)**, p145-150.

869   Merceron. T., Bonhomme, M.G., Fouillac, A.M., Vivier, G. & Meunier, A., 1987. Petrologie des

870   alterations hydrothermales du sondage GPF Echassieres n1. *Geologie de France*, **2-3**, p259-269.

871   Moissenet, M.L., 1871. Mémoire sur une nouvelle espèce minérale rencontrée dans le gîte d'étain

872   de Montebras (Creuse). Annales des Mines, **20(4)**, p1-21.

873   Moore, P.B., 1973. Pegmatites phosphates: descriptive mineralogy and crystal chemistry. *The*

874   *Mineralogical Record*, p103-130.

875   Moore, P.B., 1982. Pegmatite minerals of P(V) and B(III). *In:* P. Černý. Ed., Granitic pegmatites in

876   Science and Industry. *Mineralogical Association of Canada, Short Course Handbook*, **8**, p267-291.

877   Neiva, A. M. R., Silva, M. M. V. G., Antunes, I. M. H. R. & Ramos, J. M. F., 2000. Phosphate

878   minerals of some granitic rocks and associated quartz veins from northern and central Portugal.

879   *Journal of the Czech Geological Society*, **45(3-4)**, 4p.

880   Neiva, A. M. R. & Ramos, J. M. F., 2010. Geochemistry of granitic aplite-pegmatite sills and

881   petrogenetic links with granites, Guarda-Belmonte area, central Portugal. *European Journal of*

882   *Mineralogy*. **22**, p837-854.

883 Nicolas, J. & de Rosen, A., 1963. Phosphates hydrothermaux de basse temperature et kaolinisation:

884 la gorceixite du massif des Colettes (Allier) et les mineraux associes (hinsdalite). *Bulletin de la*

885 *Societe francaise de Mineralogie et de Cristallographie*, **86**, p379-385.

886 Pal, D.C., Biswajit, M. & Bernhardt, H. J., 2007. Mineralogy and geochemistry of pegmatite-hosted

887 Sn-, Ta-Nb- and Zr-Hf-bearing minerals from the southeastern part of the Bastar-Malkangiri

888 pegmatite belt, Central India, *Ore Geological Review*, **30**, p30-55.

889 PePiper, G. & Dolansky L. M., 2005. Early diagenetic origin of Al phosphate-sulfate minerals

890 (woodhouseite and crandallite series) in terrestrial sandstones, Nova Scotia, Canada. *American*

891 *Mineralogist*, **90**, p1434-1441.

892 Pichavant, M., Boher, M., Stenger, J-F., Aissa, M. & Charoy, B., 1987. Relations de phase des

893 granites de Beauvoir a 1 et 3 kbar H_2O-saturated conditions. *In*: Cuney, M. & Autran, A. : Geologie

894 profonde de la France: forage scientifique d'Echassieres: une cle pour la comprehension des

895 mecanismes magmatiques et hydrothermaux associes aux granites a metaux rares. *Geologie de*

896 *France*, **2**-3, p77-85.

897 Pirard, C. 2022. Characterisation of phosphate mineralogy in Montebras-en-Soumans Pegmatite,

898 Massif Central, France. *EarthArXiv*

899 Raimbault, L. & Burnol, L., 1998.The Richemont rhyolitic dyke (French Massif Central): a

900 subvolcanic equivalent of rare-metal granites. *The Canadian Mineralogist*, **36**, p265-282.

901 Roda-Robles, E., Galliski, M.A., Roquet, M.B., Hatert, F. & de Parseval, P., 2012. Phosphate

902 nodules containing two distinct assemblages in the Cema granitic pegmatite, San Luis Province,

903 Argentina: paragenesis, composition and significance. *The Canadian Mineralogist*, **50**, p913-931.

904 Scholz, R., Karfunkel, J., Bermanec, V., da Costa, G. M., Horn, A. H., Souza, L. A. C. & Bilal, E.,

905 2008. Amblygonite – Montebrasiters from Divino das Laranjeiras – Mendes Pimentel Pegmatitic

906 Swarm, Minas Gerais, Brazil. II. Mineralogy. *Romanian Journal of Mineral Deposits*, **83,** p135-

907 139.

908   Schreyer, W., 1987. Pre- and synmetamorphic metasomatism in peraluminous metamorphic rocks.

909   *Mathematical and Physical Science,* **218***,* p265-296.

910   Schwab, R.G., Herold, H., Gotz, C. & Pinto de Oliveira, N., 1990. Compounds of the crandallite

911   type: synthesis and properties of pure goyazite, gorceixite and plumbogummite. *Neues Jarhbuch fur*

912   *Mineralogie, Monatshefte*, **3**, p113-126.

913   Schwab, R.G., Mohr, J., Pimpl, T.H. & Schukov, H., 1996. About the fixation of alkali and earth-

914   alkali elements in laterites. *Geosciencias,* **10***,* 89-112.

915   Shirose, Y. & Uehara, S., 2014. Secondary phosphates in montebrasite and amblygonite from

916   Nagatare, Fukuoka Prefecture, Japan. *Journal of Mineralogical and Petrological Sciences*, **109**,

917   p103-108.

918   Spandler, C., Pettke, T. & Rubatto, D., 2011. Internal and external fluid sources for eclogite-facies

919   veins in the Monviso meta-ophiolite, Western Alps: Implications for fluid flow in subduction zones.

920   *Journal of Petrology*, **52(6)**, p1207-1236.

921   Stoffregen, R.E. & Alpers, C.N., 1987. Woodhouseite and svanbergite in hydrothermal ore deposits:

922   products of apatite destruction during advanced argilic alteration. *The Canadian Mineralogist,* **25**,

923   p201-211.

924   Sturman, B.D., Mandarino, J.A., Mrose, M.E. & Dunn, P.J., 1981. Gormanite,

925   $Fe^{2+}_3Al_6(PO_4)_4(OH)_6.2H_2O$, the ferrous analogue of souzalite, and new data for souzalite. *The*

926   *Canadian Mineralogist,* **19***,* p381-387.

927   Thomas, R., Webster, J.D. & Davidson, P., 2006. Understanding pegmatite formation: The melt and

928   fluid inclusion approach. *Mineralogical Association of Canada Short Course* **36**, Montreal, Quebec,

929   p189-210.

930   Van Riemsdijk, W.H., Weststrate, F.A. & Bolt, G.H., 1975. Evidence for a new aluminium

931   phosphate phase from reaction rate of phosphate with aluminium hydroxide, *Nature*, **257**, p473-474.

932   Vasyukova, O. & Williams-Jones, A.E., 2014. Fluoride-silicate melts immiscibility and its role in

933   REE ore formation: evidence from the Strange Lake rare metal deposit, Quebec-Labrador, Canada.

934   *Geochimica et Cosmochimica Acta*, **139**, p110-130.

935   Vasyukova, O. & Williams-Jones, A.E., 2016. The evolution of immiscible silicate and fluoride

936   melts: Implicatios for REE ore-genesis. *Geochimica et Cosmochimica Acta*, **172**, p205-224.

937   Veksler, I. V., Dorfman, A.M., Kamenetsky, M., Dulski, P. & Dingwell, D.B., 2005. Partitioning of

938   lanthanides and Y between immiscible silicate and fluoride melts, fluorite and cryolite and the

939   origin of the lanthanide tetrad effect in igneous rocks. *Geochimica et Cosmochimica Acta*, **69(11)**,

940   p2847-2860.

941   Veksler, I. V., Dorfman, A.M., Dulski, P., Kamenetsky, V. S., Danyushevsky, L. V., Jeffries, T. &

942   Dingwell, D. B., 2012. Partitioning of elements between silicate melt and immiscible fluoride,

943   chloride, carbonate, phosphate and sulfate melts, with implications to the origin of natrocarbonatite.

944   *Geochimica et Cosmochimica Acta*, **79**, p20-40.

945   Webster, J.D., 1990. Partitioning of F between H2O ± CO2 fluids and topaz rhyolite melt:

946   Implications for mineralizing magmatic-hydrothermal fluids in F-rich granitic systems.

947   *Contributions to Mineralogy and Petrology*, **104**, p424-438.

948   Webster, J.D., Thomas, R., Rhede, D., Forster, H.-J. & Seltmann, R., 1997. Melt inclusions in quarz

949   from an evolved peraluminous pegmatite: Geochemical evidence for strong tin enrichment in

950   fluorine-rich and phosphorus-rich residual liquids. *Geochimica et Cosmochimica Acta,* **61(13)**,

951   p2589-2604.

952   Wyllie, P.J. & Tuttle O.F., 1961. Experimental investigation of silicate system containing two

953   volatile components. Part II. The effects of NH_3 and HF in addition to H_2O on the melting

954   temperatures of albite and granite. *American Journal of Science*, **259**, p128-143.